Contact Interactions in Higgs-Vector Boson Associated Production at the ILC

Jonathan Cohen,[1,*] Shaouly Bar-Shalom,[1,†] and Gad Eilam[1,‡]

[1]*Physics Department, Technion-Institute of Technology, Haifa 32000, Israel*

(Dated: October 7, 2016)

We explore new physics (NP) effects in Higgs-Vector boson associated production at a future International Linear Collider (ILC) via $e^+e^- \to Zh\,, Zhh$, using effective field theory (EFT) techniques. In particular, we focus on a certain class of dimension 6 operators, which are generated by tree-level exchanges of a new heavy vector field in the underlying theory. These operators induce new contact terms of the form $\psi\psi\phi D\phi$, involving the Standard Model (SM) fermions (ψ), gauge-bosons (D is the covariant derivative) and the SM Higgs field (ϕ). We investigate the high-energy behaviour of these new effective interactions in $e^+e^- \to Zh\,, Zhh$, imposing bounds from electroweak precision measurements, and show that the ILC is an excellent testing ground for probing this type of NP via $e^+e^- \to Zh\,, Zhh$. We also address the validity of the EFT expansion and we study the correlation between the hZ and hhZ signals, which can be utilized in future searches for NP in these channels.

arXiv:1602.01698v3 [hep-ph] 6 Oct 2016

I. INTRODUCTION

The SM is by now a well established theory and has been tested with an astounding accuracy. Nonetheless, since the SM does not address some of the fundamental theoretical issues in particle physics, such as the hierarchy problem, dark matter, neutrino masses, flavor and CP violation, it is widely believed that the NP which underlies the SM is around the corner, i.e., at the few TeV scale. This has driven physicists throughout the years to search for new theories beyond the SM, which, in many cases, predict the existence of new particles.

In this paper we investigate NP effects in Higgs - Vector boson associated production at a future e^+e^- collider, via $e^+e^- \to hZ$ [1, 2] and $e^+e^- \to hhZ$ [3]. These processes are sensitive to a variety of underlying NP scenarios. Of the many examples in the literature, let us briefly mention studies of Higgs - Vector boson associated production processes in Little Higgs models with T parity [4], in supersymmetry where the $e^+e^- \to hZ$ cross-section receives one-loop corrections which are sensitive to the stop mass [5] and in models of extra compact dimensions, in which strong gravitational interactions at the TeV scale lead to virtual exchange of KK gravitons that affect hhZ production at the ILC [6]. The $e^+e^- \to hhZ$ cross-section can also be modified in Two Higgs doublet models (2HDM) and in models with scalar leptoquarks due to enhanced one-loop corrections to the triple Higgs coupling [7].

Over the years, the grueling task of the search for NP beyond the SM, also involved model-independent studies, which utilize EFT techniques to explore new interactions among the SM particles. In this work we adopt the EFT approach and study the effects of new Higgs - Vector Boson - fermion interactions in Higgs-Vector boson associated production at the ILC via the processes $e^+e^- \to Zh\,, Zhh$, see Fig. 1. We parameterize the new effective interactions through higher-dimensional operators assuming that:

- The new interactions obey the gauge symmetries of the SM: $SU(3)_C \times SU(2)_L \times U(1)_Y$.
- The underlying NP is weakly coupled, renormalizable and decoupled from the SM at low energies.
- The light fields, i.e., the observable degrees of freedom below the cutoff Λ (see below), are the SM fields.

Within this EFT setup the SM is treated as a low-energy effective theory and the new interactions are characterized by a new scale $\Lambda \gg v$, which represents the scale (threshold) of the NP. The effective theory is then described by:

$$\mathcal{L} \;=\; \mathcal{L}_{SM} + \sum_n \frac{f_i^{(n)}}{\Lambda^{n-4}} \mathcal{O}_i^{(n)} \;, \tag{1}$$

where i denotes the operator type, n is its dimension and $f_i^{(n)}$ are the corresponding Wilson coefficients.

*Electronic address: jcohen@tx.technion.ac.il
†Electronic address: shaouly@physics.technion.ac.il
‡Electronic address: eilam@physics.technion.ac.il

In principle, the $\mathcal{O}_i$'s are generated by integrating out the heavy fields in the underlying theory; the different types of operators then depend on the quantum numbers of the exchanged heavy fields. Thus, a generic EFT is, by construction, valid up to the scale Λ (of the NP), so that by performing a measurement in a future collider one can extract information on the ratio $f_i^{(n)}/\Lambda^{n-4}$ and, therefore, hope to find clues regarding the underlying theory [8–15] (for a comprehensive analysis of the renormalization of the dimension 6 operators and its importance for precision studies of the SM EFT framework in (1), see [16–20]). In that respect, we note that, under the assumption that the underlying NP is weakly coupled, the dimensionless coefficients $f_i^{(n)}$ in the underlying theory are expected to be of $\mathcal{O}(1)$.

In this work we limit ourselves to dimension 6 operators, $\mathcal{O}_i^{(6)}$, which contain the SM fields and derivatives, assuming that they represent the leading NP effects.[1] In particular, we consider a class of operators, which, following the notation in [10], will be denoted symbolically as the $\psi^2\varphi^2 D$ class. These operators contain a pair of fermions (ψ), two Higgs fields (Φ) and a SM covariant derivative (D) and are generated by new heavy vector-boson exchanges in Higgs-fermion systems.

Consider for example the case where a new heavy vector singlet field V'_μ, with a mass $M \gg v$, is added to the SM lagrangian (the heavy vector can be thought of as some $U(1)'$ remnant of a higher broken symmetry). The lagrangian piece for V'_μ then reads:

$$\mathcal{L} = -\frac{1}{4}V'_{\mu\nu}V'^{\mu\nu} + \frac{1}{2}M^2 V'_\mu V'^{\mu} + V'_\mu\left(gi\Phi^\dagger \overleftrightarrow{D}^\mu \Phi + \tilde{g}\bar{\psi}\gamma^\mu\psi\right) , \tag{2}$$

where, the "Hermitian derivative" in (2) is defined as $\Phi^\dagger \overleftrightarrow{D}_\mu \Phi \equiv \Phi^\dagger D_\mu \Phi - D_\mu \Phi^\dagger \Phi$.

Integrating out the heavy field V'_μ, by using its Equation of Motion (EOM), we can express V'_μ in terms of the SM light fields:

$$V'_\mu = -\frac{1}{(\Box - M^2)}\left(g\Phi^\dagger \overleftrightarrow{D}^\mu \Phi + \tilde{g}\bar{\psi}\gamma^\mu\psi\right) , \tag{3}$$

so that, performing the propagator expansion:

$$\frac{1}{(\Box - M^2)} \underbrace{\approx}_{\Box \ll M^2} -\frac{1}{M^2}\sum_{k=0}^{\infty}\left(\frac{\Box}{M^2}\right)^k , \tag{4}$$

and keeping only the first term, i.e, $k = 0$, we obtain:

$$V'_\mu \underbrace{\approx}_{\Box \ll M^2} \frac{1}{M^2}\left(g\Phi^\dagger \overleftrightarrow{D}^\mu \Phi + \tilde{g}\bar{\psi}\gamma^\mu\psi\right) . \tag{5}$$

Plugging now V'_μ in (5) back into the original lagrangian of (2), we obtain the NP Lagrangian piece which emerges from the heavy vector-boson exchange:[2]

$$\Delta\mathcal{L}_{V'} = \frac{f_{V'}}{\Lambda^2}\mathcal{O}_{V'} , \tag{6}$$

where $f_{V'} = g\tilde{g}$, $\Lambda = M$ and $\mathcal{O}_{V'}$ is the dimension 6 heavy vector singlet operator:

$$\mathcal{O}_{V'} = i\bar{\psi}\gamma^\mu\psi\Phi^\dagger \overleftrightarrow{D}^\mu \Phi . \tag{7}$$

In the case of a heavy vector triplet, one similarly obtains the operator:

$$\mathcal{O}_{\tilde{V}'} = i\bar{\psi}\sigma^k\gamma^\mu\psi\Phi^\dagger\sigma^k \overleftrightarrow{D}^\mu \Phi . \tag{8}$$

---

[1] We will henceforth drop the subscript $n = 6$ for the dimension 6 operators $\mathcal{O}_i^{(6)}$.

[2] Note that integrating out the heavy vector field in (2) will also induce new effective four-fermion contact operators. The effects of such 4-Fermion operators are not relevant for the Higgs-Vector boson production processes $e^+e^- \to Zh\,, Zhh$, and will, therefore, not be considered here.

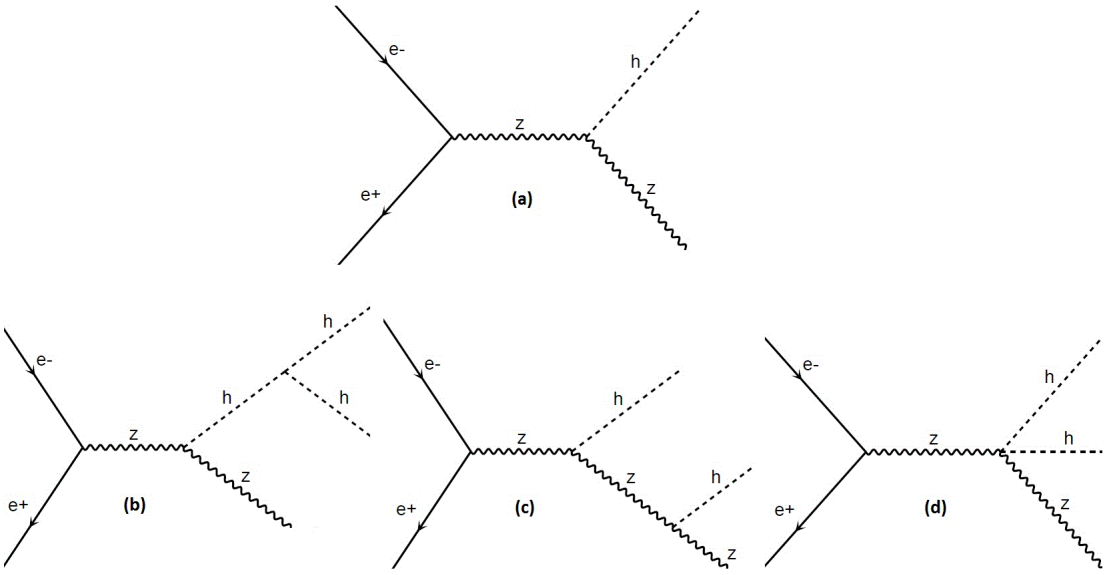

FIG. 1: Tree-level SM diagrams for $e^+e^- \to Z \to hZ$ (a) and for $e^+e^- \to Z \to hhZ$ (b,c,d).

Such $\psi^2\varphi^2 D$ operators give rise to new contact interactions of the form $l\bar{l}hZ$ and $l\bar{l}hhZ$ at scales lower than the typical new heavy particle mass (see Appendix A) and, thus, contribute to the Higgs-Vector boson associated production process $e^+e^- \to hZ,\ hhZ$ of interest in this work. Examples of Beyond the SM (BSM) constructions which involve new heavy vector fields that can underly the $\psi^2\varphi^2 D$ class operators include TeV-scale Z' models (see e.g., [21, 22]), whose origin can be related to the breaking of grand unified theories based on $SO\,(10)$ or E_6 symmetries, which may leave one or several $U\,(1)$ remnants unbroken down to TeV energies, before the symmetry is further broken to the SM symmetry. Left-Right twin Higgs models [23] also introduce new heavy gauge bosons, extra Higgs bosons and a top partner which can also affect the production of hZ and hhZ.

Similar contact interactions are also obtained for the $\psi^2\varphi^2 D$ operators involving quarks ($\psi = q$), i.e, $q\bar{q}hZ$, $q\bar{q}hhZ$, as well as contact interactions involving the W: $\overline{u}dhW$, $\overline{u}dhhW$. These may affect Higgs - Vector boson associated production at the LHC and we leave that to a future work. Nonetheless, it is worth mentioning that Higgs-Vector boson associated production is the third most dominant Higgs production channel at the LHC after gluon-gluon fusion and vector boson fusion [24]. It has been found that operators containing derivative interactions can modify the kinematic distributions in Higgs Vector-boson associated production at the LHC [25].

Note that other observables/processes can be utilized at the LHC to probe the leptonic contact interactions $l\bar{l}hZ$ and $l\bar{l}hhZ$, which are generated by the $\psi^2\varphi^2 D$ operators. For example, differential distributions in the Higgs 3-body decay $h \to Zl^+l^-$ [26–28] and the total Z-width [29] may be useful for this purpose. Nonetheless, as we will show here, a much higher sensitivity to these leptonic contact terms can be obtained at a future ILC, via $e^+e^- \to hZ, hhZ$. In particular, an ILC will be able to probe the scale of the $\psi^2\varphi^2 D$ class operators, ranging from a few TeV to $\mathcal{O}(10)$ TeV, depending upon its design (center of mass energy and luminosity).

Indeed, we wish to emphasize the underlying reasons and motivation for our choice of the $\psi^2\varphi^2 D$ class of dim. 6 operators: 1. These operators are tree-level generated in the theory only by new heavy vector-boson exchanges and are, therefore, unique in that sense - probing a certain type of new physics which can be characterized by a single heavy scale Λ. 2. These operators give rise to new contact interactions of the form $eehZ$ and $eehhZ$ which will, therefore, give an effect proportional to $(E/\Lambda)^2$ in $\sigma(e^+e^- \to hhZ, hhZ)$, where E is the c.m. energy of the process. They are, therefore, expected to give the dominant higher dimensional EFT effect in $e^+e^- \to hhZ, hhZ$, under the assumption of a weakly interacting underlying physics (i.e., with respect to other possible dim. 6 operators that can contribute to these processes).

The paper is organized as follows: in sections II we discuss the Higgs Effective Lagrangian (HEL) framework and list the current bounds from LEP/EW precision data on the $\psi^2\varphi^2 D$ class operators. In section III we give a short overview of Higgs - Vector boson associated production at the ILC. In sections IV and V we present analytical and some benchmark numerical results of the cross-sections for the processes $e^+e^- \to hZ$ and $e^+e^- \to hhZ$ in the presence of the $\psi^2\varphi^2 D$ class operators. In section V we also discuss the correlation between the hZ and the hhZ cross-sections as well as the validity of the EFT expansion. In section VI we present a more realistic analysis of the sensitivity to the $\psi^2\varphi^2 D$ class operators, based on a more realistic background (BG) estimation. In section VII we

summarize. Appendix A gives the Feynman rules associated with the $\psi^2\varphi^2 D$ class operators and Appendix B contains intermediate steps of the analytic calculation of $\sigma(e^+e^- \to hhZ)$. In Appendices C and D we depict the tree-level Feynman diagrams corresponding to hZ and hhZ signals, respectively, after the Z-decays to a pair of fermions, which were calculated for the realistic BG estimation.

II. HIGGS EFFECTIVE LAGRANGIAN - GENERAL SETUP AND CONSTRAINTS

In dealing with higher dimensional operators one often encounters non trivial Lorentz structures. An efficient way to systematically extract all the Feynman rules goes through a Mathematica package software called FeynRules (FR) [30]. We have therefore used the Higgs Effective Lagrangian (HEL) implementation in FR of [31]. Moreover, the output from the HEL implementation in FR is readable by the event generator software MadGraph 5 (MG5) [32], which further facilitates our analysis, allowing us to perform MG5 simulations in a straightforward manner.

The HEL setup of [31] is defined by:

$$\mathcal{L} = \mathcal{L}_{SM} + \sum \bar{c}_i \mathcal{O}_i \equiv \mathcal{L}_{SM} + \mathcal{L}_{SILH} + \mathcal{L}_{F_1} + \mathcal{L}_{F_2} + \mathcal{L}_G \,, \tag{9}$$

where $\mathcal{L}_{SILH}$ (SILH=Strongly Interacting Light Higgs) is inspired by scenarios where the Higgs field is part of a strongly interacting sector, $\mathcal{L}_{F_2}$ contains interactions among a pair of fermions with a single Higgs field and a gauge-boson that originate from different NP scenarios (other than the heavy vector exchanges), $\mathcal{L}_G$ contains new gauge-boson self-interactions and $\mathcal{L}_{F_1}$ contains the $\psi^2\varphi^2 D$ class operators of our interest in (7) and (8). It is given by:

$$\begin{aligned}
\mathcal{L}_{F_1} \;=\; & \frac{i\bar{c}_{HQ}}{v^2}\left[\overline{Q}_L\gamma^\mu Q_L\right]\left[\Phi^\dagger \overleftrightarrow{D}_\mu \Phi\right] + \frac{4i\bar{c}'_{HQ}}{v^2}\left[\overline{Q}_L\gamma^\mu T_{2k} Q_L\right]\left[\Phi^\dagger T_2^k \overleftrightarrow{D}_\mu \Phi\right] \\
& + \frac{i\bar{c}_{Hu}}{v^2}\left[\overline{u}_R\gamma^\mu u_R\right]\left[\Phi^\dagger \overleftrightarrow{D}_\mu \Phi\right] + \frac{i\bar{c}_{Hd}}{v^2}\left[\overline{d}_R\gamma^\mu d_R\right]\left[\Phi^\dagger \overleftrightarrow{D}_\mu \Phi\right] - \left[\frac{i\bar{c}_{Hud}}{v^2}\left[\overline{u}_R\gamma^\mu d_R\right]\left[\Phi \cdot \overleftrightarrow{D}_\mu \Phi\right] + h.c.\right] \\
& + \frac{i\bar{c}_{HL}}{v^2}\left[\overline{L}_L\gamma^\mu L_L\right]\left[\Phi^\dagger \overleftrightarrow{D}_\mu \Phi\right] + \frac{4i\bar{c}'_{HL}}{v^2}\left[\overline{L}_L\gamma^\mu T_{2k} L_L\right]\left[\Phi^\dagger T_2^k \overleftrightarrow{D}_\mu \Phi\right] + \frac{i\bar{c}_{He}}{v^2}\left[\overline{e}_R\gamma^\mu e_R\right]\left[\Phi^\dagger \overleftrightarrow{D}_\mu \Phi\right],
\end{aligned} \tag{10}$$

where $Q_L = \begin{pmatrix} u_L \\ d_L \end{pmatrix}$, u_R and d_R are the three generations of left-handed and right-handed quark fields, respectively and the corresponding lepton fields are $L_L = \begin{pmatrix} \nu_L \\ l_L \end{pmatrix}$ and e_R. Also, T_{2k} are the $SU(2)$ generators in the fundamental representation, $T_{2k} = \frac{\sigma_k}{2}$, where σ_k are the Pauli matrices.

Furthermore, the coefficients $\bar{c}_i$ are normalized such that they are related to f_i in (1) by

$$\bar{c}_i = \frac{v^2}{\Lambda^2} f_i \,, \tag{11}$$

In general, if one writes down all possible dimension 6 operators consistent with the SM symmetries (which exhibit baryon and lepton number conservation), one arrives to a finite number of operators. However, the SM EOM along with the use of integration by parts and field redefinitions may result in a redundancy of this description. That is, some of the operators may be equivalent, up to total derivatives, to linear combinations of other operators [13]. Indeed, as has been advocated in both [10] and [31], the $\psi^2\varphi^2 D$ class operators, as they appear in $\mathcal{L}_{F_1}$, are equivalent (using the EOM's) to linear combinations of some purely bosonic operators in $\mathcal{L}_{SILH}$, and can, therefore, be eliminated by trading them with these bosonic operators; the choice of basis may vary depending on the analysis one wishes to carry out, see for example [33, 34]. This might be part of the reason why the effects of these $\psi^2\varphi^2 D$ operators have not been thoroughly studied. Moreover, the bosonic operators are loop generated in the underlying theory (see [13]), so that their contribution is expected in general to be further suppressed, typically by a factor of $1/16\pi^2$ (recall that the $\psi^2\varphi^2 D$ class operators are generated by tree-level exchanges of heavy vector-bosons in the underlying theory).

Here we will follow the GIMR basis of [10], which explicitly includes the $\psi^2\varphi^2 D$ class operators in (7) and (8), which we seek to explore in this work. In particular, we will be interested in the leptonic operators corresponding to $\bar{c}_{HL}$, $\bar{c}'_{HL}$ and $\bar{c}_{He}$, which can affect the hZ and hhZ signals, $e^+e^- \to hZ, hhZ$, at the ILC. These leptonic operators and, in general all the $\psi^2\varphi^2 D$ class operators, are tightly constrained by Z-pole measurements, as they modify its vector and axial-vector couplings to a pair of fermions. Indeed, a fit to ElectroWeak (EW) precision data [35] has

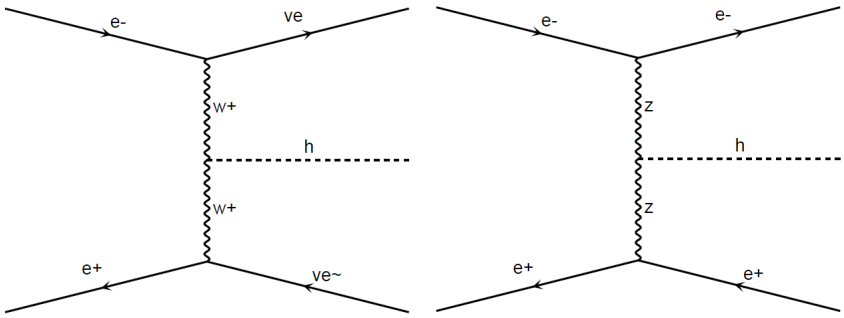

FIG. 2: Tree-level SM diagrams for the WW-fusion process $e^+e^- \to h\nu\overline{\nu}$ (left) and ZZ-fusion process $e^+e^- \to he^+e^-$ (right).

been performed in [36] to yield the following bounds on the Wilson coefficients of the leptonic operators:[3]

$$\begin{aligned} -0.0003 < \ & \bar{c}_{HL} + \bar{c}'_{HL} \ < 0.002 \\ -0.002 < \ & \bar{c}_{HL} - \bar{c}'_{HL} \ < 0.004 \\ -0.0009 < \ & \bar{c}_{He} \ < 0.003 \ . \end{aligned} \tag{12}$$

The bounds in (12) can be translated into bounds on the ratio's f_i/Λ^2 through (11). In practice, the upper (lower) bounds in (12) correspond to $f_i > 0$ ($f_i < 0$). In what follows we always set for simplicity $f_i = 1$ or $f_i = -1$ and use Λ as the only unknown with respect to the NP. For example using the one coupling scheme for $\bar{c}_{HL}$:

$$-0.0003 < \bar{c}_{HL} < 0.002 \, , \tag{13}$$

the above upper and lower bounds correspond to $\Lambda \gtrsim 5.5$ TeV and $\Lambda \gtrsim 14$ TeV, for $f_{HL} = 1$ and $f_{HL} = -1$, respectively. Similarly, in the one parameter scheme for $\bar{c}_{He}$, we obtain $\Lambda \gtrsim 4.5$ TeV and $\Lambda \gtrsim 8$ TeV, for $f_{He} = 1$ and $f_{He} = -1$, respectively.

III. HIGGS - VECTOR BOSON ASSOCIATED PRODUCTION AT THE ILC - A SHORT OVERVIEW

The future planned ILC, although having a lower energy reach, provides a cleaner environment, as it doesn't suffer from the large QCD background which is typical to hadron colliders. Moreover, the center of mass energy at an ILC ($\sqrt{s}$) is precisely known and it also provides the possibility of polarizing the colliding electron beams. The cross-sections of the main Higgs production modes at the ILC are given for example in [37].

Clearly, the BG for the process $e^+e^- \to hZ$ depends on the subsequent decays of Z and h. In the case of $Z \to \nu\overline{\nu}$ the leading BG is the WW-fusion process shown in Fig. 2, while for the case where $Z \to e^+e^-$,i.e., $e^+e^- \to hZ \to he^+e^-$, the leading BG is the ZZ-fusion process also shown in Fig. 2 (see e.g., [38]). Both the WW and ZZ-fusion processes grow logarithmically with $\sqrt{s}$, the ZZ fusion being about 10 times smaller than the WW-fusion one due to the different strengths between the W and the Z couplings to electrons. In that respect, let us mention [39], where a study of the dimension 6 operators $\mathcal{O}_H$ and $\mathcal{O}_6$ in $\mathcal{L}_{SILH}$ (see [31]), which affect the WWh, ZZh and hhh couplings in $e^+e^- \to hZ \to (anything)(l^+l^-)$ was performed. They reconstructed the Higgs mass using the recoil mass + acceptance cuts technique (see [40]) and imposed additional cuts, such as the invariant mass cut $|m_Z - \mathcal{M}(ll)| < 10$ GeV, to further reduce the BG for the hZ signal. This allows, for example, to reduce the effective number of BG events for $e^+e^- \to hZ \to b\bar{b}l^+l^-$, coming from u and t channel electron exchange in $e^+e^- \to ZZ \to b\bar{b}l^+l^-$, to about 10% of the signal (see also [41]).

Indeed, as we will show below, the $hZ \to hf\overline{f}$ final state can be distinguished from the gauge-boson fusion BG processes through an appropriate set of cuts and choice of final states. For example, the contribution of $\mathcal{O}_{He}, \mathcal{O}_{HL}, \mathcal{O}_{HL'}$ from the interference with the SM can be substantial in the $hf\overline{f}$ channel with $f = \mu, \tau$ or q, i.e., giving rise to a correction of more than 5% (20%) at a center of mass energy of $\sqrt{s} = 500$ GeV (1 TeV). On the other hand, the

[3] The bounds on the $\psi^2\varphi^2 D$ operators involving the light(heavy)-quarks are comparable(weaker) to those on the leptonic operators in (12).

relative impact of $\mathcal{O}_{He}, \mathcal{O}_{HL}, \mathcal{O}_{HL'}$ on he^+e^- and $h+\not{E}$ is smaller, since these signals suffer from the large WW-fusion and ZZ-fusion BG.

As mentioned earlier, an important feature of the future planned ILC is the possibility of polarizing the incoming electron-positron, which can be straightforwardly utilized for various purposes. For example, for hZ production followed by Z decay to neutrinos, one can "switch off" the WW fusion contribution by choosing right-handed electrons (and left-handed positrons) [42]. The SM cross-sections for $e^+e^- \to Z \to hZ$ including initial state polarization effects can be found in [24].

The process $e^+e^- \to hZ$ at the ILC, in the presence of the contact terms which are generated by the $\psi^2\varphi^2 D$ class operators, was initially considered in [43] and was found to show significant deviations from the SM by choosing a combination of operators which saturates the bounds on the corresponding Wilson coefficients, i.e, maximizing the statistical significance. Later on, [44] expanded the analysis of [43] by looking at angular distributions in $e^+e^- \to hZ \to h\overline{f}f$. Recently, Craig *et al.* in [5] have also considered the effects of the $\psi^2\varphi^2 D$ class operators in $e^+e^- \to hZ$ at an ILC with a center of mass energy of $\sqrt{s}$ =250 GeV, taking into account only the interferences with the SM (i.e. only the corrections of order $1/\Lambda^2$, see next section). They found that the exclusion/discovery potential (of such a machine) to the scale these operators, which heavily relies on the accuracy of the measurement, is $\Lambda \sim$ few TeV [5].

As for $e^+e^- \to hhZ$ (see Fig. 1), its cross-section peaks at about 0.18 [fb] close to $\sqrt{s}$ =500 GeV and then drops as $1/s$ at high energies. On of the main motivations for measuring $e^+e^- \to hhZ$ is the feasibility of detecting the trilinear Higgs coupling λ (see diagram (b) in Fig. 1), though there are other important diagrams that do not contain λ but still contribute to hhZ (see diagrams (c) and (d) in Fig. 1). This results in a dilution of $\frac{\Delta\lambda}{\lambda} \simeq 1.75\frac{\Delta\sigma_{hhZ}}{\sigma_{hhZ}}$ at $\sqrt{s}$ =500 GeV, where $\Delta\lambda$ ($\Delta\sigma$) are the measured accuracies [45], [46]. The sensitivity to the Higgs self coupling in $e^+e^- \to hhZ$ has, therefore, been a subject of intense study throughout the years [47–50].

A primary example of an EFT analysis of hhZ production at the ILC was given in [51], where dimension 6 operators that give rise to anomalous Higgs self-couplings were considered. They found that, at $\sqrt{s}$ =800 GeV, the normalized $p_T(Z)$ distribution and the hh invariant mass distribution (in $e^+e^- \to hhZ$) exhibit dramatic differences from the SM ones in the presence of the new effective anomalous Higgs self-couplings. A similar analysis, also involving CP violating effective operators, has been performed for $e^+e^- \to hW^+W^-$ in [52].

IV. $e^+e^- \to hZ$ & $e^+e^- \to hhZ$ - ANALYTICAL ANALYSIS

In this section we present an analytical derivation of the cross-sections for the processes $e^+e^- \to hZ$ and $e^+e^- \to hhZ$ in the presence of the $\psi^2\varphi^2 D$ class operators[4].

A. $e^+e^- \to hZ$

The SM diagram leading to $e^+e^- \to hZ$ appears in Fig. 1(a), while the NP contributions to $e^+e^- \to hZ$ induced by the $\psi^2\varphi^2 D$ class operators $\mathcal{O}_{HL}, \mathcal{O}'_{HL}$ and $\mathcal{O}_{He}$ (in $\mathcal{L}_{F1}$) are depicted in Fig. 3. Summing up the contributions from all orders (i.e. in the $\left(1/\Lambda^2\right)$ expansion) we obtain

$$\sigma(hZ) \;=\; \sigma_{SM}(hZ)\left(1+\frac{\delta_1(s,f_i)}{\Lambda^2}+\frac{\delta_2(s,f_i)}{\Lambda^4}\right)\,, \tag{14}$$

where

$$\sigma_{SM}(hZ) \;=\; \frac{\alpha m_Z^2}{12v^2}\frac{\left(a_e^2+v_e^2\right)}{\left(s-m_Z^2\right)^2}w\left(w^2+\frac{12m_Z^2}{s}\right)\,, \tag{15}$$

$$w=\sqrt{\left(1-\frac{m_h^2}{s}-\frac{m_Z^2}{s}\right)^2-\frac{4m_h^2m_Z^2}{s^2}}\,, \tag{16}$$

and the $\mathcal{O}(1/\Lambda^2)$ and $\mathcal{O}(1/\Lambda^4)$ corrections are:

---

[4] We note that loop effects from the EFT are expected to be suppressed by at least a factor of $1/16\pi^2$ and, in some cases, by an additional factor of $(v/\sqrt{s})^2$, compared to the dominant tree-level contributions from the new contact terms. Their effect are, therefore, not important for the purpose of our investigation and they have a negligible effect on the results shown below (i.e., on the sensitivity plots to the scale of the new physics).

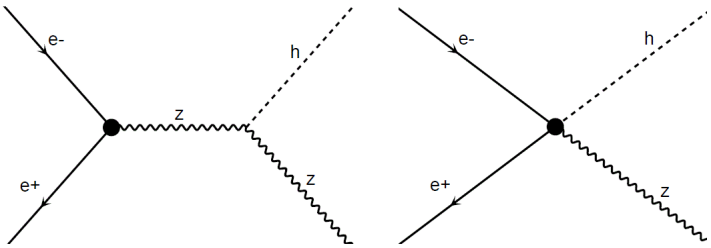

FIG. 3: Tree-level diagrams for $e^+e^- \to h\,Z$ in the presence of the $\psi^2\varphi^2 D$ operators, due to a shift in Z coupling to leptons (left) and due to the $eehZ$ contact term (right). The relevant Feynman rules are given in Appendix A.

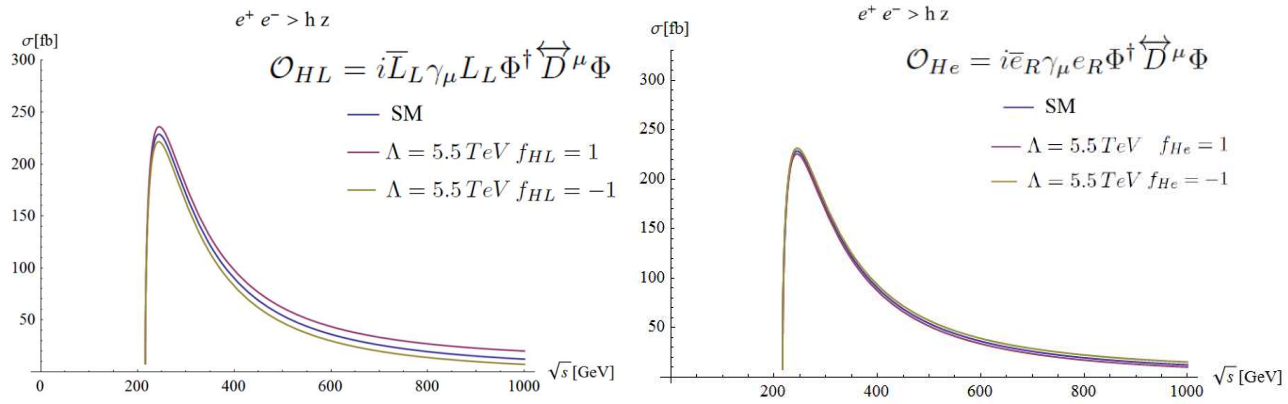

FIG. 4: $\sigma(e^+e^- \to hZ)$ as a function of the center of mass energy in the presence of $\mathcal{O}_{HL}$ (left figure) and $\mathcal{O}_{He}$ (right figure). The operator $\mathcal{O}'_{HL}$ has the same effect as $\mathcal{O}_{HL}$ since the amplitude is $\propto (f_{HL} + f'_{HL})$.

$$\delta_1(s, f_i) = \frac{s}{2c_W s_W}\frac{a_e\left[(f_{HL}+f'_{HL}) - \frac{f_{He}}{2}\right] + v_e\left[(f_{HL}+f'_{HL}) + \frac{f_{He}}{2}\right]}{a_e^2 + v_e^2}\frac{v^2}{M_Z^2}\,, \tag{17}$$

$$\delta_2(s, f_i) = \left(\frac{s}{4c_W s_W}\right)^2 \frac{\left[(f_{HL}+f'_{HL}) - \frac{f_{He}}{2}\right]^2 + \left[(f_{HL}+f'_{HL}) + \frac{f_{He}}{2}\right]^2}{a_e^2 + v_e^2}\left(\frac{v^2}{M_Z^2}\right)^2\,. \tag{18}$$

Note that, as expected, the interference of the contact term with the SM diagram grows with energy, i.e. the term $\propto \frac{\delta_1}{\Lambda^2}$. For consistency matters, we included the term $\propto \frac{\delta_2}{\Lambda^4}$, which corresponds to the squared amplitude of the contact interaction NP diagram in Fig. 3 and which is, therefore, expected to be small when $\sqrt{s} < \Lambda$ (i.e., compared to the leading $\mathcal{O}\left(\frac{\delta_1}{\Lambda^2}\right)$ term). All other terms cancel out when taking the sum of all contributions.

The term $\propto \frac{\delta_2}{\Lambda^4}$ is, however, a vital ingredient of the full squared amplitude, as it formally ensures a positive cross-section. The case where the $\mathcal{O}\left(\frac{\delta_2}{\Lambda^4}\right)$ "correction" becomes comparable to the SM signifies the point where the validity of our current EFT framework breaks and the necessity of considering higher dimensional operators (i.e., in our case, dimension 8 ones). We will return to this point later.

In Fig. 4 we plot $\sigma(e^+e^- \to hZ)$ as a function of $\sqrt{s}$, where we switch on one operator at a time (setting all others to zero). In particular, we set $\Lambda = 5.5$ TeV for both $f_{HL}, f_{He} = \pm 1$. The operator $\mathcal{O}'_{HL}$ has the same effect as $\mathcal{O}_{HL}$ since the amplitude is $\propto (f_{HL} + f'_{HL})$. We see that the cross-section is less sensitive to $\mathcal{O}_{He}$, for $\Lambda = 5.5$ TeV, partly since f_{He} appears to have an extra suppression factor of 2 w.r.t f_{HL} in the cross-section, see (17) and (18).

B. $e^+e^- \to hhZ$

As for the process $e^+e^- \to hhZ$, the SM diagrams leading to $e^+e^- \to hhZ$ are shown in Fig. 1(b),(c),(d), while the NP diagrams corresponding to the $\psi^2\varphi^2 D$ class operators are plotted in Fig. 5. In particular, there are two types of

new contributions: a shift in the Z coupling to leptons and the new contact terms $eehZ$ and $eehhZ$. The NP diagrams

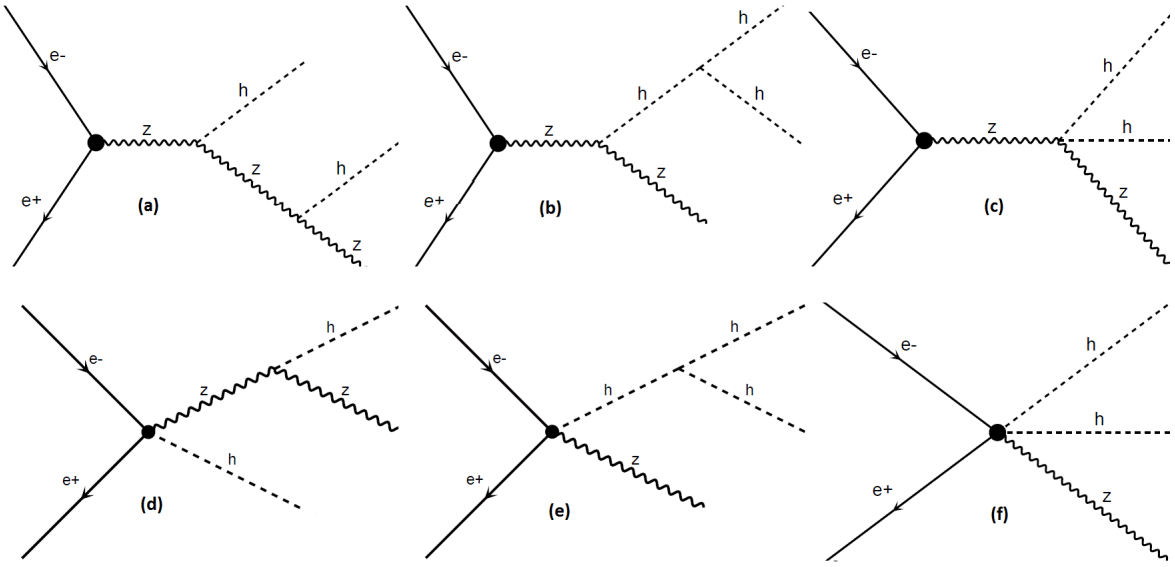

FIG. 5: Diagrams for $e^+e^- \to hhZ$ in the presence of $\psi^2\varphi^2 D$ class operators.

exhibit similar patterns as the three SM ones, so that we can express them in terms of the SM one. Moreover, the expansions in $1/\Lambda^2$ exactly coincides with the one given above for the $e^+e^- \to hZ$ case, allowing us to conveniently write the total squared amplitude as:

$$|\mathcal{M}|^2 \;=\; |\mathcal{M}_{SM}|^2 \left(1 + \frac{\delta_1\left(s, f_i\right)}{\Lambda^2} + \frac{\delta_2\left(s, f_i\right)}{\Lambda^4}\right) \;, \tag{19}$$

where δ_1 and δ_2 are given in (17) and (18), respectively, and $|\mathcal{M}_{SM}|^2$ is given in appendix B. The differential cross-section is

$$d\sigma \;=\; \frac{1}{2}\frac{1}{2s}\frac{1}{\left(2\pi\right)^5}\frac{1}{4}\sum |\mathcal{M}|^2\,\delta^4\left(\left(-l_1\right) + l_2 - p_3 - p_4 - p_5\right)\frac{d^3p_3}{2E_3}\frac{d^3p_4}{2E_4}\frac{d^3p_5}{2E_5}\,, \tag{20}$$

where $(-l_1, l_2)$ denote the (e^+, e^-) momenta and (p_3, p_4, p_5) denote the (h, h, z) momenta (the extra 1/2 factor which accounts for the two identical particles hh in the final state is explicitly factored out).

As will be shown below, the resemblance between the hZ and hhZ expansions at the level of the matrix element squared in the presence of our $\psi^2\phi^2 D$ class operators, may be come handy for the study of NP in $e^+e^- \to hZ, hhZ$.

V. $e^+e^- \to hZ$ & $e^+e^- \to hhZ$ - NUMERICAL ANALYSIS

A. Naive sensitivities and benchmark values

Let us define

$$N_{SD}\left(\sqrt{s}, f_i, \Lambda\right) \;\equiv\; \frac{N^T - N^{SM}}{\sqrt{N^T}}\;, \tag{21}$$

where N_{SD} is the statistical significance of the signal, σ^T (σ^{SM}) is the cross-section in the presence of the new effective operators (in the SM), $N^{T,SM} = \sigma^{T,SM}L$ is the corresponding total number of events and $L = \int \mathcal{L}dt$ is the integrated luminosity, which may vary, depending on the given center of mass energy and design of the ILC. In particular, we have performed MADGRAPH simulations (using MG5 [32]) for both $e^+e^- \to hZ$ and $e^+e^- \to hhZ$, in

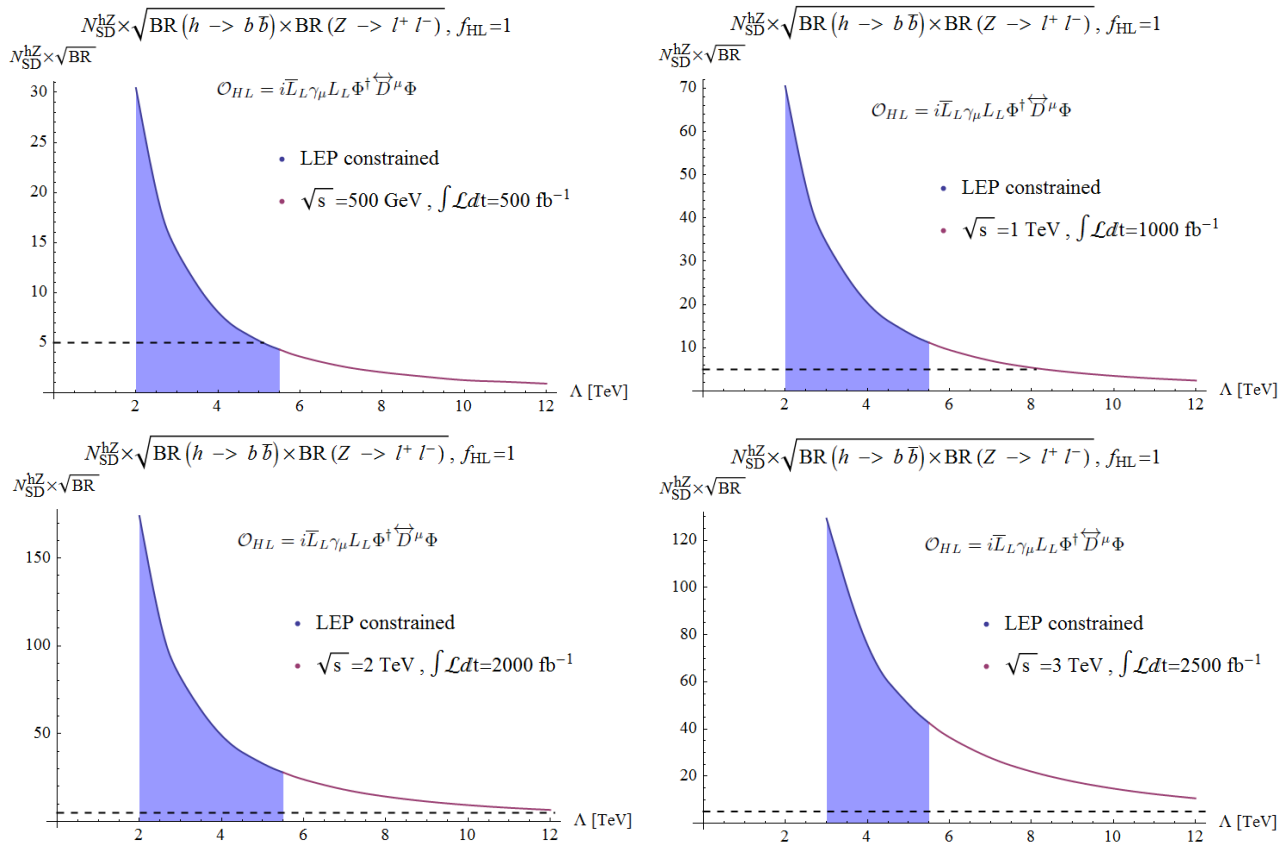
$N_{SD}^{hZ}\times\sqrt{BR\,(h\ ->\ b\,\bar{b})\times BR\,(Z\ ->\ l^+\,l^-)}$, f_{HL}=1
$N_{SD}^{hZ}\times\sqrt{BR}$
$\mathcal{O}_{HL}=i\bar{L}_L\gamma_\mu L_L\Phi^\dagger\overleftrightarrow{D}^\mu\Phi$
LEP constrained
$\sqrt{s}$ =500 GeV , $\int\mathcal{L}dt$=500 fb^{-1}
$\sqrt{s}$ =1 TeV , $\int\mathcal{L}dt$=1000 fb^{-1}
$\sqrt{s}$ =2 TeV , $\int\mathcal{L}dt$=2000 fb^{-1}
$\sqrt{s}$ =3 TeV , $\int\mathcal{L}dt$=2500 fb^{-1}
Λ [TeV]

FIG. 6: Sensitivity to the NP scale (Λ) for $e^+e^- \to hZ \to b\bar{b}l^+l^-$ at $\sqrt{s} = 500$ GeV with $L = 500\,fb^{-1}$, $\sqrt{s} = 1$ TeV with $L = 1000\,fb^{-1}$, $\sqrt{s} = 2$ TeV with $L = 2000\,fb^{-1}$ and $\sqrt{s} = 3$ TeV with $L = 2500\,fb^{-1}$. The blue region is constrained by LEP. The dashed horizontal line is the naive 5σ sensitivity.

the presence of $\mathcal{O}_{HL}$ - using the HEL model implementation of [31] in MG5 - at an ILC with the benchmark designs [37]: $\left\{\sqrt{s}\ [\text{TeV}], L\ [\text{fb}^{-1}]\right\} = \{0.5, 500\}, \{1, 1000\}, \{2, 2000\}, \{3, 2500\}$.

In Fig. 6 we show the expected sensitivity N_{SD} as a function of Λ for the hZ signal, where we examine the specific decay mode of the hZ final state $h \to b\bar{b}$ and $Z \to l^+l^-$, with $l^\pm = e^\pm, \mu^\pm$ (we sum over the electrons and muons final states, i.e., $l^+l^- = e^+e^- + \mu^+\mu^-$), by multiplying the number of events $N^{T,SM}$ with the corresponding SM Branching Ratios (BRs): $BR\left(h \to b\bar{b}\right) \sim 60\%$ and $BR\left(Z \to l^+l^-\right) = BR\left(Z \to e^+e^-\right) + BR\left(Z \to \mu^+\mu^-\right) \sim 6.8\%$. We see, for instance, that a 1 TeV ILC will be sensitive to the NP scale (associated with the $\psi^2\phi^2D$ operator $\mathcal{O}_{HL}$) $\Lambda \simeq 6$ TeV at the $\sim 10\sigma$ level, in the channel $hZ \to b\bar{b}l^+l^-$ (efficiencies such as b-tagging, etc. are not included). As can be seen, at larger center of mass energies the effect of $\mathcal{O}_{HL}$ is more pronounced. As for hhZ production, we find no sensitivity to $\mathcal{O}_{HL}$ when $\Lambda > 5.5$ TeV (which is the LEP bound on this operator) at an ILC with $\sqrt{s} = 500$ GeV and $\sqrt{s} = 1$ TeV, where the total number of events is $N^T < 10$. We, therefore, show in Fig. 7 the sensitivity plots for the hhZ signal only in the case where the center of mass energy is $\sqrt{s} = 2$ TeV and 3 TeV. We see that, for the 2 TeV ILC, a 5σ effect can be obtained for the signal $hhZ \to b\bar{b}b\bar{b}l^+l^-$ if $\Lambda = 4$ TeV. The sensitivity reach is extended to $\Lambda \sim 8$ TeV at a $\sqrt{s} = 3$ TeV machine, a 5σ effect is plausible in the case $hhZ \to b\bar{b}b\bar{b}l^+l^-$ for $\Lambda = 5.5$ TeV.

In Table 3.1 we summarize the highlights of the analysis presented in this section.

B. Validity of the EFT expansion

Let us further define the "validity" function, $\mathcal{R}$:

$$\mathcal{R} \equiv \frac{\Delta\sigma_2}{\sigma_1}, \tag{22}$$

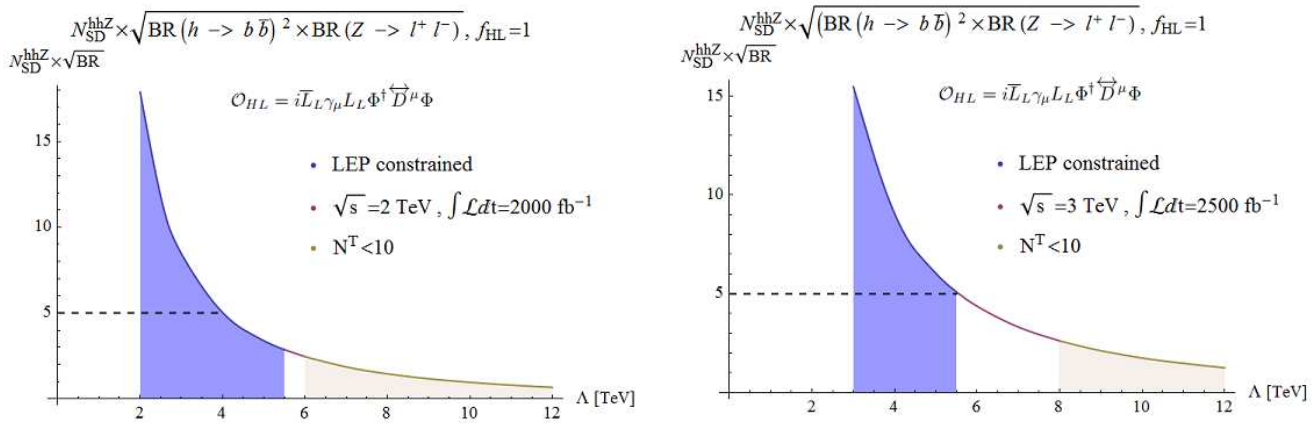

FIG. 7: Sensitivity to NP (Λ) for $e^+e^- \to hhZ \to b\bar{b}b\bar{b}l^+l^-$ at $\sqrt{s} = 2$ TeV with $L = 2000\,fb^{-1}$ (left plot) and $\sqrt{s} = 3$ TeV with $L = 2500\,fb^{-1}$ (right plot). The dark blue region is constrained by LEP. The shaded brown region has $N^T < 10$. In between lies a "window of opportunity" for Λ. The dashed horizontal line is the naive 5σ sensitivity.

$e^+e^- \to hZ \to b\bar{b} + l^+l^-$				
$\sqrt{s}$	500 GeV	1 TeV	2 TeV	3 TeV
$\Lambda >$	5 TeV	8 TeV	12 TeV	$\gtrsim$ 14 TeV

$e^+e^- \to hhZ \to b\bar{b} + b\bar{b} + l^+l^-$		
$\sqrt{s}$	2 TeV	3 TeV
$\Lambda >$	4 TeV	5.5 TeV

TABLE I: 5σ reach on Λ for each ILC design: naive estimates for hZ production (upper table) and hhZ production (lower table), followed by the Higgs decay to $b\bar{b}$ and the Z decay to leptons.

where

$$\Delta\sigma_2 \ \equiv\ \frac{\delta_2\,(s,f_i)}{\Lambda^4}\,,\ \sigma_1 \equiv 1+\frac{\delta_1\,(s,f_i)}{\Lambda^2}\,,$$

in accordance with the expansion used for the hZ and hhZ cross-sections, see (14). That is, $\Delta\sigma_2$ corresponds to the square of the NP amplitude.

In Fig. 8 we examine the validity functions $\mathcal{R}$ as a function of the scale of NP, Λ, for both hZ and hhZ production in the presence of $\mathcal{O}_{HL}$ and for all center of mass energies under consideration. The similarity between the validity functions for the hZ and hhZ signals, shown in Fig. 8, is a consequence of the resemblance of the expansions in $1/\Lambda^2$ that was found in the previous section for the corresponding cross-sections (see also below). We see that the $1/\Lambda^4$ correction term $\Delta\sigma_2$ exceeds the $1/\Lambda^2$ interference term, i.e., giving $\mathcal{R} > 1$, as we go to lower values of Λ (in which case s/Λ^2 increases). We consider all values of Λ that lie above the dashed line $\mathcal{R} = 1$ in Fig. 8 to be inconsistent with our EFT expansion to dimension 6 operators. This is prompted from our ignorance of the value of $\Delta\sigma_2$, as it is subject to corrections from dimension 8 operators which we didn't consider in our analysis. In particular, dimension 8 operators in the expansion

$$\mathcal{L}\ =\ \mathcal{L}_{SM}+\sum_i\frac{f_i^{(6)}}{\Lambda^2}\mathcal{O}_i^{(6)}+\sum_j\frac{f_j^{(8)}}{\Lambda^4}\mathcal{O}_i^{(8)}+\cdots \tag{23}$$

may contribute to the $eehZ$ and/or $eehhz$ contact interactions through their interference with the SM diagrams, yielding a contribution of the same order $(1/\Lambda^4)$ as $\Delta\sigma_2$.

A natural dimension 8 operator, $\mathcal{O}_i^{(8)}$, that comes to mind is $\Phi^\dagger\Phi\times\mathcal{O}_{HL}$, which contributes to the same contact interactions but with a small suppression factor of v^2/Λ^2 and is, thus, negligible. Another interesting dimension 8 operator arises from the propagator expansion in (4) from the $k = 1$ term, yielding the same $\psi^2\varphi^2 D$ class operators

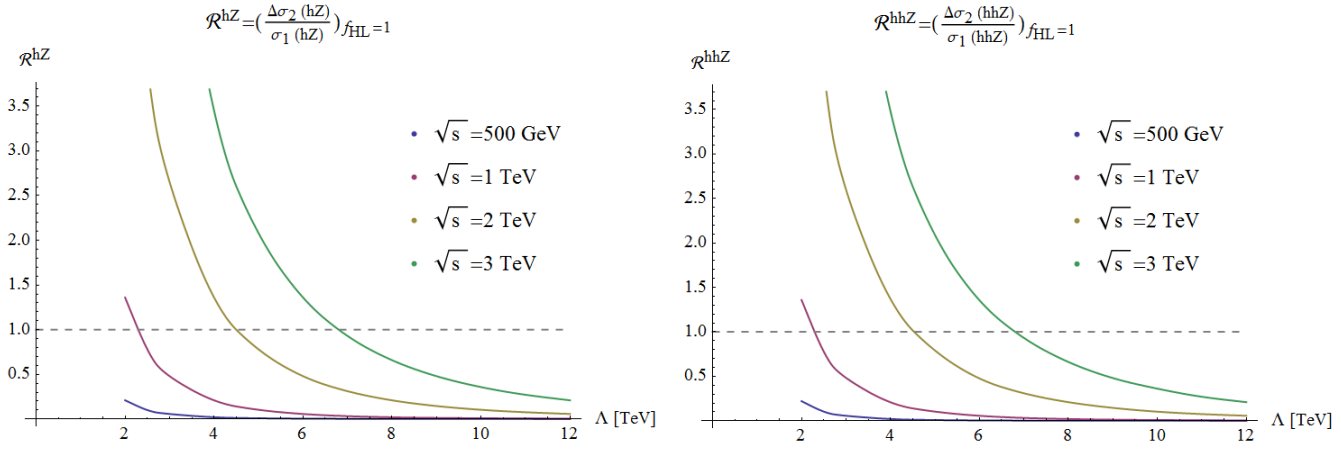

FIG. 8: Validity functions $\mathcal{R}^{hZ} \equiv \frac{\Delta\sigma_2\left(e^+e^-\to hZ\right)}{\sigma_1\left(e^+e^-\to hZ\right)}$ (left plot) and $\mathcal{R}^{hhZ} \equiv \frac{\Delta\sigma_2\left(e^+e^-\to hhZ\right)}{\sigma_1\left(e^+e^-\to hhZ\right)}$ (right plot), as a function of Λ for all energies under consideration.

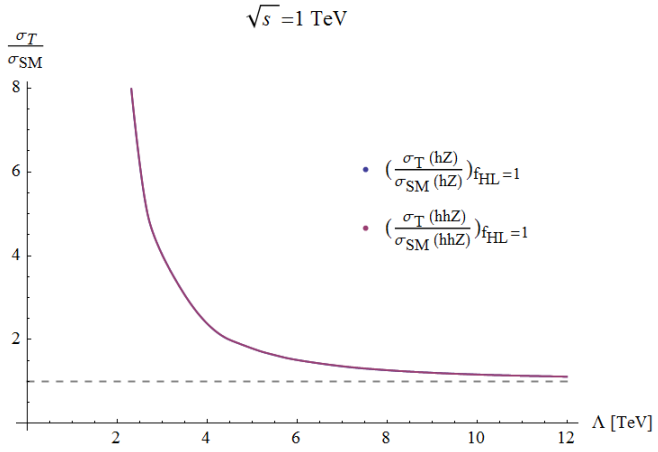

FIG. 9: $\left(\frac{\sigma^T}{\sigma^{SM}}\right)_{f_{HL}=1}$ for $e^+e^-\to hZ$ and $e^+e^-\to hhZ$, at $\sqrt{s}=1$ TeV.

but with extra higher derivatives. That is, the operator $i\bar{\psi}\gamma^\mu\psi\Box\Phi^\dagger\overleftrightarrow{D}_\mu\Phi$, which, in the case of $\mathcal{R}>1$, may play an important role.

C. An $hZ-hhZ$ Correlation

Using the results of section IV, we plot in Fig. 9 the ratio $\frac{\sigma^T}{\sigma^{SM}}$ as a function of Λ, in the presence of the operator $\mathcal{O}_{HL}$, for both the hZ and hhZ signals at a 1 TeV ILC. As expected, we find $\frac{\sigma^T(hZ)}{\sigma^{SM}(hZ)} = \frac{\sigma^T(hhZ)}{\sigma^{SM}(hhZ)}$, which holds for any center of mass energy. This validates numerically the similarity of the expansions in $1/\Lambda^2$ for $\sigma^T\left(e^+e^-\to hZ\right)$ and $\sigma^T\left(e^+e^-\to hhZ\right)$ that was found in the analytic derivation of section IV.

This property could play a key role in distinguishing between different NP scenarios. For example anomalous Higgs self-couplings are expected to exhibit a different behavior in $e^+e^-\to hZ$ versus $e^+e^-\to hhZ$.

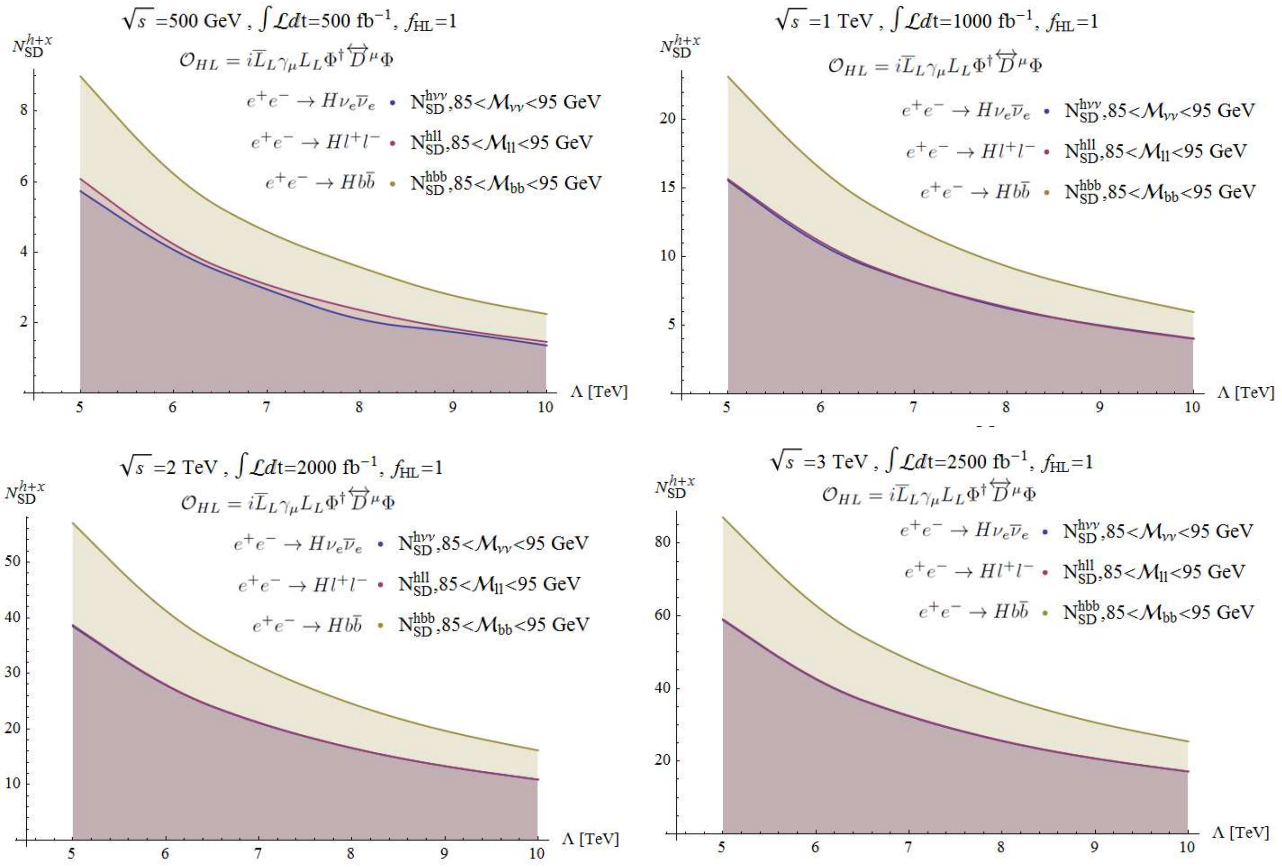
$\sqrt{s}$ =500 GeV , $\int \mathcal{L}dt$=500 fb^{-1}, f_{HL}=1
$\mathcal{O}_{HL} = i\bar{L}_L\gamma_\mu L_L\Phi^\dagger \overleftrightarrow{D}^\mu\Phi$
$e^+e^- \to H\nu_e\bar{\nu}_e$ • $N_{SD}^{h\nu\nu}$,85<$\mathcal{M}_{\nu\nu}$<95 GeV
$e^+e^- \to Hl^+l^-$ • N_{SD}^{hll},85<$\mathcal{M}_{ll}$<95 GeV
$e^+e^- \to Hb\bar{b}$ • N_{SD}^{hbb},85<$\mathcal{M}_{bb}$<95 GeV
N_{SD}^{h+x}
Λ [TeV]
$\sqrt{s}$ =1 TeV , $\int \mathcal{L}dt$=1000 fb^{-1}, f_{HL}=1
$\sqrt{s}$ =2 TeV , $\int \mathcal{L}dt$=2000 fb^{-1}, f_{HL}=1
$\sqrt{s}$ =3 TeV , $\int \mathcal{L}dt$=2500 fb^{-1}, f_{HL}=1

FIG. 10: Sensitivity (N_{SD}) to the NP scale Λ, for $e^+e^- \to hZ \to h\nu_e\bar{\nu}_e, hl^+l^-, hb\bar{b}$, at $\sqrt{s} = 500$ GeV with $L = 500\, fb^{-1}$, $\sqrt{s} = 1$ TeV with $L = 1000\, fb^{-1}$, $\sqrt{s} = 2$ TeV with $L = 2000\, fb^{-1}$ and $\sqrt{s} = 3$ TeV with $L = 2500\, fb^{-1}$.

VI. REALISTIC BACKGROUND ESTIMATION AND SENSITIVITIES

In this section we present a realistic calculation of the signal to BG ratio for $e^+e^- \to hZ, hhZ$, including all possible diagrams that are generated by the SM + $\psi^2\varphi^2 D$ type operators. We note again that possible effects from diagrams containing EFT insertions of other dim. 6 operators (e.g., effective triple Higgs couplings) are expected to be much smaller, than the leading SM + $\psi^2\varphi^2 D$ contribution (for a fixed value of Λ) and are, therefore, neglected in both signal and BG calculation.

A. $e^+e^- \to hZ$

Let us consider the process $e^+e^- \to hZ$ followed by $Z \to \nu_e\bar{\nu}_e, l^+l^-, b\bar{b}$ in the presence of $\mathcal{O}_{HL}$, taking into account all the possible signal+BG diagrams which lead to $e^+e^- \to h\nu_e\bar{\nu}_e, hl^+l^-, hb\bar{b}$. As before, we sum over the electrons and muons final states ($l^+l^- = e^+e^- + \mu^+\mu^-$) in both the signal and BG calculations. In particular, there are 16 diagrams in the $h\nu_e\bar{\nu}_e$ channel, 24 diagrams in the hl^+l^- channel and 18 diagrams in $hb\bar{b}$ channel, all depicted in Appendix C. We impose kinematical cuts to suppress the BG (in particular the WW and ZZ-fusion processes) and perform a more realistic estimate of the sensitivity to the $\psi^2\varphi^2 D$ operators in $e^+e^- \to hZ \to h\nu_e\bar{\nu}_e, hl^+l^-, hb\bar{b}$.

For example, for the he^+e^- final state, we reject most of the BG from the ZZ-fusion process (see Fig. 2), by imposing a cut on the invariant mass of the e^+e^- system to lie within $m_Z - 2\Gamma_Z < \mathcal{M}_{ee} < m_Z + 2\Gamma_Z$, together with the acceptance cuts $p_T(e) > 15$ GeV, $p_T(ee) > 80$ GeV.

Our results for the case of $e^+e^- \to h\nu_e\bar{\nu}_e$ are shown in Table II, where we also compare the naive cross-section estimates of section V [i.e., $\sigma(e^+e^- \to h\nu_e\bar{\nu}_e) \approx \sigma(e^+e^- \to hZ) \times \mathcal{BR}(Z \to \nu_e\bar{\nu}_e)$] with the full cross-section calculation, including all diagrams and imposing the appropriate invariant-mass cut to reduce the WW-fusion BG. Evidently, our naive estimates hold even in the presence of the irreducible BG, indicating that the WW-fusion BG has been

$e^+e^- \to h\nu_e\overline{\nu}_e$ comparison with naive estimates of section 3.1						
	$\sqrt{s}$=500 GeV			$\sqrt{s}$=1 TeV		
	Before cuts	After cuts	$\sigma_{hZ} \times \mathcal{BR}_Z$	Before cuts	After cuts	$\sigma_{hZ} \times \mathcal{BR}_Z$
σ^{SM} [fb]	757	3.64	3.74	205.7	0.7874	0.840
$\left(\sigma^T\right)_{\Lambda=6\,TeV}$ [fb]	759	4.029	4.16	206.7	1.182	1.127

	$\sqrt{s}$=2 TeV			$\sqrt{s}$=3 TeV		
	Before cuts	After cuts	$\sigma_{hZ} \times \mathcal{BR}_Z$	Before cuts	After cuts	$\sigma_{hZ} \times \mathcal{BR}_Z$
σ^{SM} [fb]	374.9	0.1889	0.203	483.6	0.0834	0.0898
$\left(\sigma^T\right)_{\Lambda=6\,TeV}$ [fb]	376	0.7574	0.8190	485.8	0.9561	1.03

TABLE II: SM and SM+NP cross-sections in the $e^+e^- \to h\nu_e\overline{\nu}_e$ channel including all SM and NP diagrams, after imposing the cut on the missing invariant mass of the two neutrinos $m_Z - 4\Gamma_Z < \mathcal{M}_{\nu_e\overline{\nu}_e} < m_Z + 4\Gamma_Z$ (in order to suppress the WW-fusion BG, see Fig. 2 and Appendix C). Also shown are the corresponding naive cross-sections of section V: $\sigma_{hZ} \times \mathcal{BR}_Z$, where $\sigma_{hZ} \equiv \sigma\left(e^+e^- \to hZ\right)$ and $\mathcal{BR}_Z \equiv \mathcal{BR}\left(Z \to \nu_e\overline{\nu}_e\right) = 6.6\%$. Results are given for $\sqrt{s}$=500 GeV, 1 TeV (upper table) and 2 ,3 TeV (lower table). For the NP cross-section we take Λ =6 TeV.

$\sqrt{s}$	N_{SD}^{hll} , $N_{SD}^{h\nu\nu}$	Λ
500 GeV	6σ	5 TeV
1 TeV	10σ	6 TeV
2 TeV	20σ	7 TeV
3 TeV	25σ	8 TeV

$\sqrt{s}$	N_{SD}^{hbb}	Λ
500 GeV	6σ	6 TeV
1 TeV	10σ	8 TeV
2 TeV	20σ	9 TeV
3 TeV	25σ	10 TeV

TABLE III: The expected sensitivity on the scale of NP, Λ, for selected values of N_{SD}^{hll} , $N_{SD}^{h\nu\nu}$ (left table) and N_{SD}^{hbb} (right table), see also text.

significantly reduced.

We note that the $h\nu_e\overline{\nu}_e = h + \not{E}_T$ signal is of particular interest since it resembles dark matter (DM) searches in both e^+e^- machines, see e.g., [53, 54], and at the LHC, see e.g., [55]. For example, if the DM interacts via a Higgs portal operator $\chi^2\Phi^2$ (where χ =DM and Φ is the SM Higgs doublet), then the production of an off-shell Higgs via $gg \to h^* \to h\,\chi\overline{\chi}$ will gives rise to the $h + \not{E}_T$ signature at the LHC [55].

As in section V, we plot in Fig. 10 the sensitivity, N_{SD}, as a function of the scale of the NP scale Λ, for the three proposed scenarios/decay modes: $hZ \to h\nu_e\overline{\nu}_e, hl^+l^-, hb\bar{b}$. The $hb\bar{b}$ channel is expected to have a higher sensitivity to Λ since it doesn't suffer from WW/ZZ-fusion BG (see the corresponding diagrams in Appendix C), see also [56]. The neutrino and lepton channels (blue and red respectively) exhibit the same behaviour, albeit, with a lower sensitivity than the $b\bar{b}$ channel (yellow). In particular, we see that, at a 1 TeV collider, the $h + \not{E}_T$ channel (neutrino channel) is sensitive to $\Lambda = 6$ TeV at a $\sim 10\sigma$ level, whereas the $hb\bar{b}$ channel will reach this sensitivity (10σ) for a higher NP threshold of $\sim \Lambda = 8$ TeV.

In Table III we list some selected realistic results for the expected sensitivity of the ILC to the scale of NP, Λ, in $e^+e^- \to hZ \to h\nu_e\overline{\nu}_e, hl^+l^-, hb\bar{b}$.

B. $e^+e^- \to hhZ$

We repeat the same analysis for the hhZ signals $e^+e^- \to hhZ \to hh\nu_e\overline{\nu}_e, hhl^+l^-, hhb\bar{b}$ at $\sqrt{s} = 3$ TeV, taking into account all SM+NP diagrams and imposing similar kinematical cuts to reduce the BG. There are ~ 100 diagrams for the hhl^+l^- and $hhb\bar{b}$ channels and ~ 70 diagrams for the $hh\nu_e\overline{\nu}_e$ channel; a sample of these diagrams is shown in Appendix D.

Our results for the $e^+e^- \to hhZ \to hh\nu_e\overline{\nu}_e, hhl^+l^-, hhb\bar{b}$ cases are shown in Fig. 11. We see that the difference between the $hh\nu_e\overline{\nu}_e$ and hhl^+l^- signals (blue and red, respectively) is more pronounced in the case of the Higgs pair production channel $e^+e^- \to hhZ$ (than the single Higgs production one $e^+e^- \to hZ$). Also, as in the case of hZ production, the $hhb\bar{b}$ channel (yellow) is more sensitive than the leptonic channels to the scale of the NP Λ. In fact, in the case of the lepton channels, $hh\nu_e\overline{\nu}_e$ and hhl^+l^-, the results shown in Fig. 11 are very similar to our naive estimates of section V.

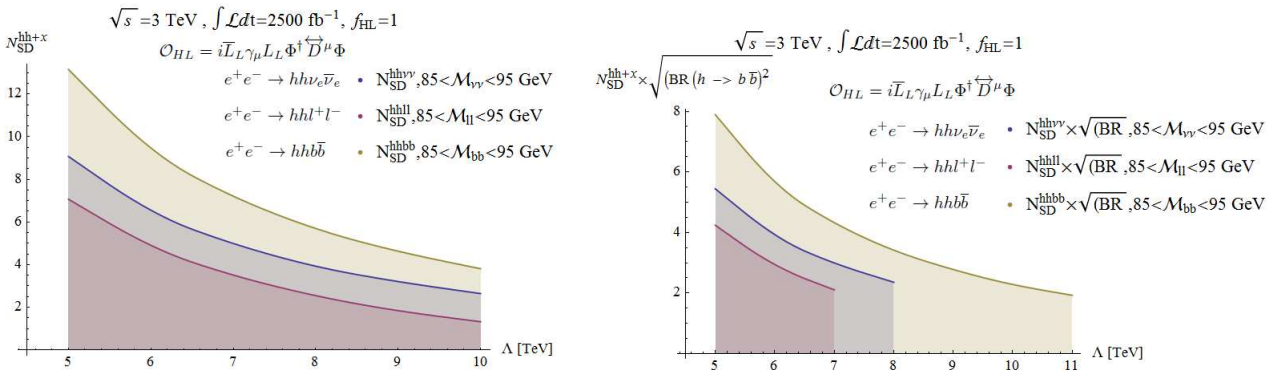
$\sqrt{s}$ =3 TeV , $\int \mathcal{L}dt$=2500 fb^{-1}, f_{HL}=1
$\mathcal{O}_{HL} = i\bar{L}_L\gamma_\mu L_L\Phi^\dagger \overleftrightarrow{D}^\mu\Phi$
$e^+e^- \to hh\nu_e\bar{\nu}_e$ • $N_{SD}^{hh\nu\nu}$,85<$\mathcal{M}_{\nu\nu}$<95 GeV
$e^+e^- \to hhl^+l^-$ • N_{SD}^{hhll},85<$\mathcal{M}_{ll}$<95 GeV
$e^+e^- \to hhb\bar{b}$ • N_{SD}^{hhbb},85<$\mathcal{M}_{bb}$<95 GeV
N_{SD}^{hh+x}
Λ [TeV]
$\sqrt{s}$ =3 TeV , $\int \mathcal{L}dt$=2500 fb^{-1}, f_{HL}=1
$N_{SD}^{hh+x}\times\sqrt{(BR\,(h \to b\bar{b})^2}$
$\mathcal{O}_{HL} = i\bar{L}_L\gamma_\mu L_L\Phi^\dagger \overleftrightarrow{D}^\mu\Phi$
$e^+e^- \to hh\nu_e\bar{\nu}_e$ • $N_{SD}^{hh\nu\nu}\times\sqrt{(BR}$,85<$\mathcal{M}_{\nu\nu}$<95 GeV
$e^+e^- \to hhl^+l^-$ • $N_{SD}^{hhll}\times\sqrt{(BR}$,85<$\mathcal{M}_{ll}$<95 GeV
$e^+e^- \to hhb\bar{b}$ • $N_{SD}^{hhbb}\times\sqrt{(BR}$,85<$\mathcal{M}_{bb}$<95 GeV
Λ [TeV]

FIG. 11: Sensitivity (N_{SD}) to the NP scale Λ, at a $\sqrt{s} = 3$ TeV ILC with $L = 2500\, fb^{-1}$. Left figure: for $e^+e^- \to hhZ \to hh\nu_e\overline{\nu}_e, hhl^+l^-, hhb\overline{b}$, right figure: for $e^+e^- \to hhZ$ followed by $hh \to b\overline{b}b\overline{b}$ and $Z \to \nu_e\overline{\nu}_e, l^+l^-, b\overline{b}$, where the curves are cut when $N^T < 10$ (i.e., less than 10 events).

In Fig. 11 we also show the sensitivity for the case in which each of the Higgs in the final state further decays via $h \to b\bar{b}$, i.e., $N_{SD}^{hh+x} \times \sqrt{BR\left(h \to b\bar{b}\right)^2}$, and the corresponding reach on Λ for all Z decay channels. We omit the region excluded by LEP ($\Lambda \lesssim 5$ TeV) and the cases where there are less than 10 events, i.e., the region where $N^T < 10$. We see that, in the case of $hh \to b\bar{b}b\bar{b}$, the "window" of reach on Λ depends on the Z decay channel. In particular, when Z decays to leptons the sensitivity window reaches $\Lambda = 7$ TeV (smaller by ~ 1 TeV compared to the naive estimate of section V), whereas for the other channels the sensitivity reach on Λ extends to 8 TeV (neutrino channel) and 11 TeV ($b\bar{b}$ channel).

C. Differential Distributions

We have processed the numerical results of section V using MadAnalysis5 [57], to study some useful differential distributions in both hZ and hhZ production channels in the presence of $\mathcal{O}_{HL}$. This is shown in Fig. 12, where we see that no particular new behaviour is exhibited, in the sense that all distributions are magnified w.r.t the SM, whereas the shape of the distributions remains intact.

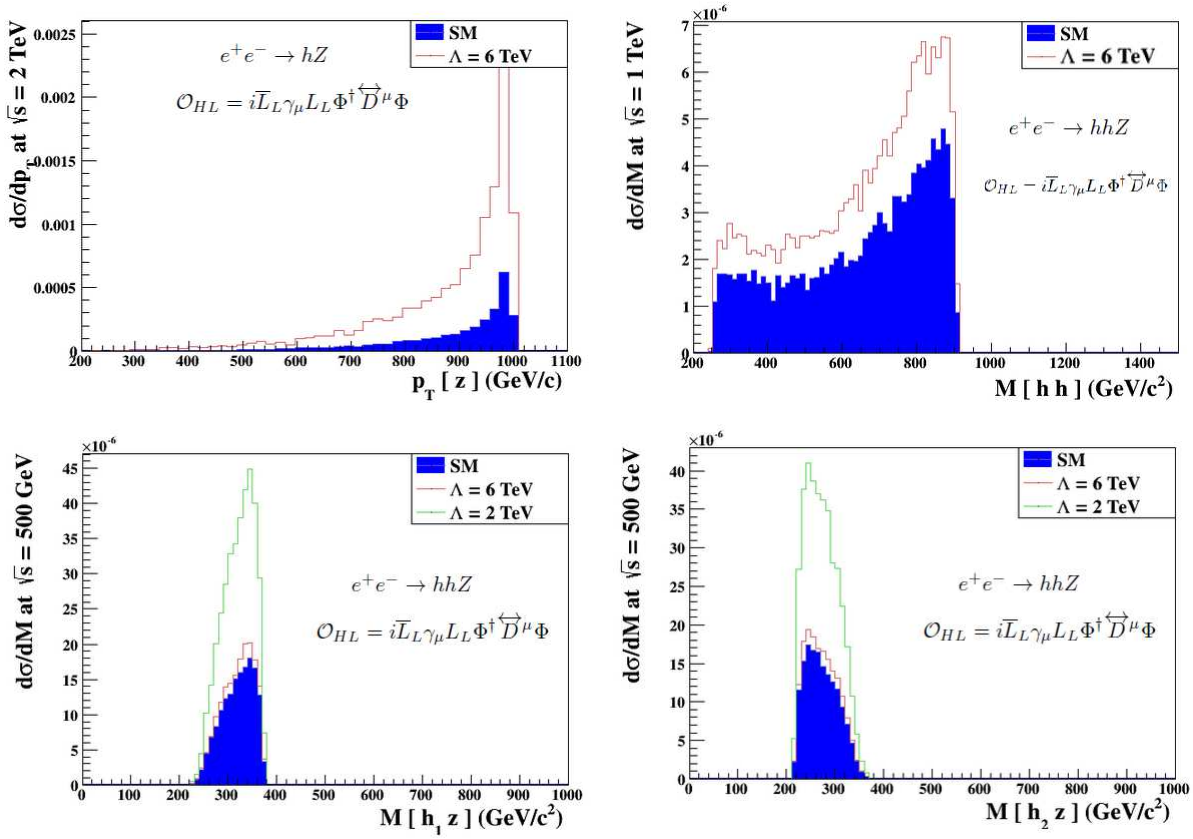
SM
Λ = 6 TeV
Λ = 2 TeV
$e^+e^- \to hZ$
$\mathcal{O}_{HL} = i\bar{L}_L\gamma_\mu L_L\Phi^\dagger\overleftrightarrow{D}^\mu\Phi$
$e^+e^- \to hhZ$
$\mathcal{O}_{HL} = i\bar{L}_L\gamma_\mu L_L\Phi^\dagger\overleftrightarrow{D}^\mu\Phi$
dσ/dp_T at √s = 2 TeV
p_T [z] (GeV/c)
dσ/dM at √s = 1 TeV
M [h h] (GeV/c²)
dσ/dM at √s = 500 GeV
M [h_1 z] (GeV/c²)
M [h_2 z] (GeV/c²)

FIG. 12: The p_T (Z) distribution in $e^+e^- \to hZ$ at $\sqrt{s}$ =2 TeV (upper left), the invariant mass distribution of hh in $e^+e^- \to hhZ$ at $\sqrt{s}$ =1 TeV (upper right), the invariant mass distribution of Z + the Higgs with the largest-p_T in $e^+e^- \to hhZ$ at $\sqrt{s}$ =500 GeV (lower left) and the invariant mass of Z + the Higgs with the 2nd largest-p_T in $e^+e^- \to hhZ$ at $\sqrt{s}$ =500 GeV (lower right). The blue-solid histogram depicts the SM predictions while the red (green) solid lines correspond to the total cross-section including the effect of $\mathcal{O}_{HL}$, where $f_{HL} = 1$ and $\Lambda = 6$ TeV ($\Lambda = 2$ TeV).

VII. SUMMARY

We have investigated possible NP effects in Higgs - Vector boson associated production at a future ILC in a model independent approach, using a certain class of dimension 6 operators - the $\psi^2\varphi^2 D$ class operators, where ψ is a fermion, φ is the SM Higgs field and D is the SM covariant derivative. These operators are generated by new heavy vector-boson exchanges at high energy scales $\Lambda \gg v$ in the underlying theory and they give rise to new contact interactions of the form e^+e^-hZ and e^+e^-hhZ.

$e^+e^- \to hZ \to h + x$ for $\Lambda = 6$ TeV			
	N_{SD}^{hll}	$N_{SD}^{h\nu\nu}$	N_{SD}^{hbb}
$\sqrt{s} = 500$ GeV	4σ	4σ	6σ
$\sqrt{s} = 1$ TeV	10σ	10σ	16σ

$e^+e^- \to hhZ \to hh + x$ for $\Lambda = 7$ TeV			
	N_{SD}^{hhll}	$N_{SD}^{hh\nu\nu}$	N_{SD}^{hhbb}
$\sqrt{s} = 3$ TeV	3.5σ	5σ	7σ

TABLE IV: An example of realistic estimates for the expected statistical significance N_{SD}^{hx} for probing NP with $\Lambda = 6$ TeV in $e^+e^- \to hZ$ followed by $Z \to x$, at $\sqrt{s}$ =500 GeV, 1 TeV (upper table) and, similarly, N_{SD}^{hhx} for probing NP with $\Lambda = 7$ TeV in $e^+e^- \to hhZ$ followed by $Z \to x$, at $\sqrt{s} = 3$ TeV (lower table).

We have presented full analytical expressions of the tree-level cross-sections for $e^+e^- \to hZ$ and $e^+e^- \to hhZ$ in the presence of the $\psi^2\varphi^2 D$ class operators, and showed that they have an identical dependence in the $1/\Lambda^2$ expansion. As a result, we found an interesting correlation between the hZ and the hhZ signals which can be utilized in future NP searches in these channels.

We performed MadGraph simulations for both $e^+e^- \to hZ$ and $e^+e^- \to hhZ$ at an ILC with center of mass energies $\sqrt{s} = 500$ GeV, 1 TeV, 2 TeV and 3 TeV and obtained realistic estimates of the sensitivity to the NP scale Λ, based on the full set of SM + NP diagrams which includes the irreducible background in the cases where the Z-boson decays via $Z \to \nu_e\overline{\nu}_e, l^+l^-$ and $Z \to b\bar{b}$.

We have also considered the constraints on the $\psi^2\varphi^2 D$ class operators, primarily from LEP, since these operators modify the Z-couplings to fermions. Our results show that a TeV-scale ILC will be able to probe NP in $e^+e^- \to hZ, hhZ$ in the form of the $\psi^2\varphi^2 D$ class operators at scales beyond the LEP bounds and the LHC 14 reach. A sample of our results is given in Table IV.

Acknowledgments: We thank Amarjit Soni and Jose Wudka for useful discussions.

[1] J. D. Bjorken, Conf. Proc. **C7608021**, 1 (1976).
[2] J. R. Ellis, M. K. Gaillard, and D. V. Nanopoulos, Nucl. Phys. **B106**, 292 (1976).
[3] G. J. Gounaris, D. Schildknecht, and F. M. Renard, Phys. Lett. **B83**, 191 (1979).
[4] B. Yang, Z. Liu, N. Liu, and J. Han, Eur. Phys. J. **C74**, 3203 (2014), 1408.4295.
[5] N. Craig, M. Farina, M. McCullough, and M. Perelstein, JHEP **03**, 146 (2015), 1411.0676.
[6] N. G. Deshpande and D. K. Ghosh, Phys. Rev. **D67**, 113006 (2003), hep-ph/0301272.
[7] E. Asakawa, D. Harada, S. Kanemura, Y. Okada, and K. Tsumura, Phys. Rev. **D82**, 115002 (2010), 1009.4670.
[8] W. Buchmuller and D. Wyler, Nucl. Phys. **B268**, 621 (1986).
[9] C. Arzt, M. B. Einhorn, and J. Wudka, Nucl. Phys. **B433**, 41 (1995), hep-ph/9405214.
[10] B. Grzadkowski, M. Iskrzynski, M. Misiak, and J. Rosiek, JHEP **10**, 085 (2010), 1008.4884.
[11] E. E. Jenkins, A. V. Manohar, and M. Trott, JHEP **09**, 063 (2013), 1305.0017.
[12] S. Willenbrock and C. Zhang, Ann. Rev. Nucl. Part. Sci. **64**, 83 (2014), 1401.0470.
[13] M. B. Einhorn and J. Wudka, Nucl. Phys. **B876**, 556 (2013), 1307.0478.
[14] B. Henning, X. Lu, and H. Murayama, (2014), 1412.1837.
[15] L. Berthier and M. Trott, JHEP **05**, 024 (2015), 1502.02570.
[16] C. Grojean, E. E. Jenkins, A. V. Manohar, and M. Trott, JHEP **04**, 016 (2013), 1301.2588.
[17] E. E. Jenkins, A. V. Manohar, and M. Trott, JHEP **10**, 087 (2013), 1308.2627.
[18] E. E. Jenkins, A. V. Manohar, and M. Trott, Phys. Lett. **B726**, 697 (2013), 1309.0819.
[19] E. E. Jenkins, A. V. Manohar, and M. Trott, JHEP **01**, 035 (2014), 1310.4838.
[20] R. Alonso, E. E. Jenkins, A. V. Manohar, and M. Trott, JHEP **04**, 159 (2014), 1312.2014.
[21] P. Langacker, AIP Conf. Proc. **1200**, 55 (2010), 0909.3260.
[22] A. Gutiérrez-Rodríguez and M. A. Hernández-Ruiz, Adv. High Energy Phys. **2015**, 593898 (2015), 1506.07575.
[23] J. Han, S. Li, B. Yang, and N. Liu, Nucl. Phys. **B896**, 200 (2015), 1504.08236.
[24] S. Dawson *et al.*, Working Group Report: Higgs Boson, in *Community Summer Study 2013: Snowmass on the Mississippi (CSS2013) Minneapolis, MN, USA, July 29-August 6, 2013*, 2013, 1310.8361.
[25] J. Ellis, V. Sanz, and T. You, JHEP **07**, 036 (2014), 1404.3667.
[26] B. Grinstein, C. W. Murphy, and D. Pirtskhalava, JHEP **10**, 077 (2013), 1305.6938.
[27] G. Isidori, A. V. Manohar, and M. Trott, Phys. Lett. **B728**, 131 (2014), 1305.0663.
[28] G. Buchalla, O. Cata, and G. D'Ambrosio, Eur. Phys. J. **C74**, 2798 (2014), 1310.2574.
[29] M. Beneke, D. Boito, and Y.-M. Wang, JHEP **11**, 028 (2014), 1406.1361.
[30] A. Alloul, N. D. Christensen, C. Degrande, C. Duhr, and B. Fuks, Comput. Phys. Commun. **185**, 2250 (2014), 1310.1921.
[31] A. Alloul, B. Fuks, and V. Sanz, JHEP **04**, 110 (2014), 1310.5150.
[32] J. Alwall *et al.*, JHEP **07**, 079 (2014), 1405.0301.
[33] J. Elias-Miro, J. R. Espinosa, E. Masso, and A. Pomarol, JHEP **11**, 066 (2013), 1308.1879.
[34] A. Pomarol and F. Riva, JHEP **01**, 151 (2014), 1308.2803.
[35] M. Baak *et al.*, Eur. Phys. J. **C72**, 2205 (2012), 1209.2716.
[36] R. Contino, M. Ghezzi, C. Grojean, M. Muhlleitner, and M. Spira, JHEP **07**, 035 (2013), 1303.3876.
[37] D. M. Asner *et al.*, ILC Higgs White Paper, in *Community Summer Study 2013: Snowmass on the Mississippi (CSS2013) Minneapolis, MN, USA, July 29-August 6, 2013*, 2013, 1310.0763.
[38] T. Han, Z. Liu, Z. Qian, and J. Sayre, Phys. Rev. **D91**, 113007 (2015), 1504.01399.
[39] V. Barger, T. Han, P. Langacker, B. McElrath, and P. Zerwas, Phys. Rev. **D67**, 115001 (2003), hep-ph/0301097.
[40] ECFA/DESY LC Physics Working Group, J. A. Aguilar-Saavedra *et al.*, (2001), hep-ph/0106315.
[41] I. Anderson *et al.*, Phys. Rev. **D89**, 035007 (2014), 1309.4819.
[42] W. Kilian, M. Kramer, and P. M. Zerwas, Phys. Lett. **B373**, 135 (1996), hep-ph/9512355.
[43] B. Grzadkowski and J. Wudka, Phys. Lett. **B364**, 49 (1995), hep-ph/9502415.
[44] W. Kilian, M. Kramer, and P. M. Zerwas, Phys. Lett. **B381**, 243 (1996), hep-ph/9603409.
[45] Y. Takubo, Analysis of ZHH in the 4-jet mode, in *Linear colliders. Proceedings, International Linear Collider Workshop, LCWS08, and International Linear Collider Meeting, ILC08, Chicago, USA, Novermber 16-20, 2008*, 2009, 0901.3598.
[46] Y. Takubo, Analysis of Higgs Self-coupling with ZHH at ILC, in *8th General Meeting of the ILC Physics Subgroup Tsukuba, Japan, January 21, 2009*, 2009, 0907.0524.
[47] D. J. Miller and S. Moretti, The Triple Higgs selfcoupling at future e+ e- colliders: A Signal to background study for the standard model, in *4th Workshop of the 2nd ECFA / DESY Study on Physics and Detectors for a Linear Electron - Positron Collider Oxford, England, March 20-23, 1999*, 1999, hep-ph/0001194.
[48] C. Castanier, P. Gay, P. Lutz, and J. Orloff, (2001), hep-ex/0101028.
[49] M. Battaglia, E. Boos, and W.-M. Yao, eConf **C010630**, E3016 (2001), hep-ph/0111276.
[50] R. Contino, C. Grojean, D. Pappadopulo, R. Rattazzi, and A. Thamm, JHEP **02**, 006 (2014), 1309.7038.
[51] S. Kumar and P. Poulose, (2014), 1408.3563.
[52] S. Kumar, P. Poulose, and S. Sahoo, Phys. Rev. **D91**, 073016 (2015), 1501.03283.
[53] S. Biswas, E. Gabrielli, M. Heikinheimo, and B. Mele, JHEP **06**, 102 (2015), 1503.05836.
[54] M. A. Fedderke, T. Lin, and L.-T. Wang, (2015), 1506.05465.
[55] D. Abercrombie *et al.*, (2015), 1507.00966.

[56] M. Thomson, Eur. Phys. J. **C76**, 72 (2016), 1509.02853.
[57] E. Conte, B. Fuks, and G. Serret, Comput. Phys. Commun. **184**, 222 (2013), 1206.1599.

Appendix A: Feynman rules

The following Feynman rules corresponding to $\mathcal{L}_{F_1}$ in (10) were obtained via the HEL model implementation of [31] in FeynRules, in the physical basis by, i.e., without the Goldstone bosons $G^0, G^{\pm}$. The left and right projection operators are denoted by $P_{\pm} = \frac{1\pm\gamma_5}{2}$. Also, $e = gs_w = g'c_w$, where $s_w(c_w)$ is the sin(cos) of the Weinberg angle. The charged leptons are denoted by l and the neutrinos by ν_l ,while u_q and d_q are the up-type and down-type quarks, respectively. V^{CKM} is the CKM mixing matrix.

The Feynmann rules involving leptons read:

$$\left\{\overline{\nu}_l, l, W^{\mu+}\right\} \; : \; \frac{i\overline{c}'_{HL} e\gamma^\mu P_-}{\sqrt{2}s_w} \tag{A1}$$

$$\left\{\overline{\nu}_l, l, h, h, W^{\mu+}\right\} \; : \; \frac{i\sqrt{2}\overline{c}'_{HL} e\gamma^\mu P_-}{s_w v^2} \tag{A2}$$

$$\left\{\overline{\nu}_l, l, h, W^{\mu+}\right\} \; : \; \frac{i\sqrt{2}\overline{c}'_{HL} e\gamma^\mu P_-}{s_w v} \tag{A3}$$

$$\left\{\overline{\nu}_l, \nu_l, Z^{\mu}\right\} \; : \; -\frac{i\overline{c}_{HL} e\gamma^\mu P_-}{2s_w c_w} + \frac{i\overline{c}'_{HL} e\gamma^\mu P_-}{2s_w c_w} \tag{A4}$$

$$\left\{\overline{\nu}_l, \nu_l, h, h, Z^{\mu}\right\} \; : \; -\frac{i\overline{c}_{HL} e\gamma^\mu P_-}{s_w c_w v^2} + \frac{i\overline{c}'_{HL} e\gamma^\mu P_-}{s_w c_w v^2} \tag{A5}$$

$$\left\{\overline{\nu}_l, \nu_l, h, Z^{\mu}\right\} \; : \; -\frac{i\overline{c}_{HL} e\gamma^\mu P_-}{s_w c_w v} + \frac{i\overline{c}'_{HL} e\gamma^\mu P_-}{s_w c_w v} \tag{A6}$$

$$\left\{\overline{l}, \nu_l, W^{\mu-}\right\} \; : \; \frac{i\overline{c}'_{HL} e\gamma^\mu P_-}{\sqrt{2}s_w} \tag{A7}$$

$$\left\{\overline{l}, \nu_l, h, h, W^{\mu-}\right\} \; : \; \frac{i\sqrt{2}\overline{c}'_{HL} e\gamma^\mu P_-}{s_w v^2} \tag{A8}$$

$$\left\{\overline{l}, \nu_l, h, W^{\mu-}\right\} \; : \; \frac{i\sqrt{2}\overline{c}'_{HL} e\gamma^\mu P_-}{s_w v} \tag{A9}$$

$$\left\{\overline{l}, l, Z^{\mu}\right\} \; : \; -\frac{i\overline{c}_{HL} e\gamma^\mu P_-}{2s_w c_w} - \frac{i\overline{c}'_{HL} e\gamma^\mu P_-}{2s_w c_w} - \frac{i\overline{c}_{He} e\gamma^\mu P_+}{4s_w c_w} \tag{A10}$$

$$\left\{\overline{l}, l, h, h, Z^{\mu}\right\} \; : \; -\frac{i\overline{c}_{HL} e\gamma^\mu P_-}{s_w c_w v^2} - \frac{i\overline{c}'_{HL} e\gamma^\mu P_-}{s_w c_w v^2} - \frac{i\overline{c}_{He} e\gamma^\mu P_+}{2s_w c_w v^2} \tag{A11}$$

$$\left\{\overline{l}, l, h, Z^{\mu}\right\} \; : \; -\frac{i\overline{c}_{HL} e\gamma^\mu P_-}{s_w c_w v} - \frac{i\overline{c}'_{HL} e\gamma^\mu P_-}{s_w c_w v} - \frac{i\overline{c}_{He} e\gamma^\mu P_+}{2s_w c_w v} \tag{A12}$$

The Feynman rules involving quarks read:

$$\left\{\overline{u}_q, d_q, W^{\mu+}\right\} \ : \ \frac{i\overline{c}'_{HQ} e V^{CKM} \gamma^\mu P_-}{\sqrt{2} s_w} + \frac{i\overline{c}_{Hud} e \gamma^\mu P_+}{\sqrt{2} s_w} \tag{A13}$$

$$\left\{\overline{u}_q, d_q, h, h, W^{\mu+}\right\} \ : \ \frac{i\sqrt{2}\overline{c}'_{HQ} e V^{CKM} \gamma^\mu P_-}{s_w v^2} + \frac{i\sqrt{2}\overline{c}_{Hud} e \gamma^\mu P_+}{s_w v^2} \tag{A14}$$

$$\left\{\overline{u}_q, d_q, h, W^{\mu+}\right\} \ : \ \frac{i\sqrt{2}\overline{c}'_{HQ} e V^{CKM} \gamma^\mu P_-}{s_w v} + \frac{i\sqrt{2}\overline{c}_{Hud} e \gamma^\mu P_+}{s_w v} \tag{A15}$$

$$\left\{\overline{u}_q, u_q, Z^\mu\right\} \ : \ -\frac{i\overline{c}_{HQ} e \gamma^\mu P_-}{2 s_w c_w} + \frac{i\overline{c}'_{HQ} e \gamma^\mu P_-}{2 s_w c_w} - \frac{i\overline{c}_{Hu} e \gamma^\mu P_+}{2 s_w c_w} \tag{A16}$$

$$\left\{\overline{u}_q, u_q, h, h, Z^\mu\right\} \ : \ -\frac{i\overline{c}_{HQ} e \gamma^\mu P_-}{s_w c_w v^2} + \frac{i\overline{c}'_{HQ} e \gamma^\mu P_-}{s_w c_w v^2} - \frac{i\overline{c}_{Hu} e \gamma^\mu P_+}{s_w c_w v^2} \tag{A17}$$

$$\left\{\overline{u}_q, u_q, h, Z^\mu\right\} \ : \ -\frac{i\overline{c}_{HQ} e \gamma^\mu P_-}{s_w c_w v} + \frac{i\overline{c}'_{HQ} e \gamma^\mu P_-}{s_w c_w v} - \frac{i\overline{c}_{Hu} e \gamma^\mu P_+}{s_w c_w v} \tag{A18}$$

$$\left\{\overline{d}_q, u_q, W^{\mu-}\right\} \ : \ \frac{i\overline{c}'_{HQ} e \left(V^{CKM}\right)^* \gamma^\mu P_-}{\sqrt{2} s_w} + \frac{i\overline{c}_{Hud} e \gamma^\mu P_+}{\sqrt{2} s_w} \tag{A19}$$

$$\left\{\overline{d}_q, u_q, h, h, W^{\mu-}\right\} \ : \ \frac{i\sqrt{2}\overline{c}'_{HQ} e \left(V^{CKM}\right)^* \gamma^\mu P_-}{s_w v^2} + \frac{i\sqrt{2}\overline{c}_{Hud} e \gamma^\mu P_+}{s_w v^2} \tag{A20}$$

$$\left\{\overline{d}_q, u_q, h, W^{\mu-}\right\} \ : \ \frac{i\sqrt{2}\overline{c}'_{HQ} e \left(V^{CKM}\right)^* \gamma^\mu P_-}{s_w v} + \frac{i\sqrt{2}\overline{c}_{Hud} e \gamma^\mu P_+}{s_w v} \tag{A21}$$

$$\left\{\overline{d}_q, d_q, Z^\mu\right\} \ : \ -\frac{i\overline{c}_{HQ} e \gamma^\mu P_-}{2 s_w c_w} - \frac{i\overline{c}'_{HQ} e \gamma^\mu P_-}{2 s_w c_w} - \frac{i\overline{c}_{Hd} e \gamma^\mu P_+}{2 s_w c_w} \tag{A22}$$

$$\left\{\overline{d}_q, d_q, h, h, Z^\mu\right\} \ : \ -\frac{i\overline{c}_{HQ} e \gamma^\mu P_-}{s_w c_w v^2} - \frac{i\overline{c}'_{HQ} e \gamma^\mu P_-}{s_w c_w v^2} - \frac{i\overline{c}_{Hd} e \gamma^\mu P_+}{s_w c_w v^2} \tag{A23}$$

$$\left\{\overline{d}_q, d_q, h, Z^\mu\right\} \ : \ -\frac{i\overline{c}_{HQ} e \gamma^\mu P_-}{s_w c_w v} - \frac{i\overline{c}'_{HQ} e \gamma^\mu P_-}{s_w c_w v} - \frac{i\overline{c}_{Hd} e \gamma^\mu P_+}{s_w c_w v} \tag{A24}$$

Appendix B: $e^+e^- \to hhZ$ Intermediate Calculations

We denote the (e^+, e^-) momenta by $(-l_1, l_2)$ and the (h, h, z) momenta by (p_3, p_4, p_5). Then, all the terms in the hhZ SM amplitude squared are given by:

$$\frac{1}{4}\sum\left|\mathcal{M}^{(1)}_{SM}\right|^2 = \frac{4e^2m_Z^4\left(a_e^2+v_e^2\right)}{\left(q^2-m_Z^2\right)^2v^4}t_1\,, \tag{B1}$$

$$\frac{1}{4}\sum\left|\mathcal{M}^{(2)}_{SM}\right|^2 = \frac{16e^2m_Z^8\left(a_e^2+v_e^2\right)}{v^4\left(q^2-m_Z^2\right)^2}\left(d_1^2t_1+\frac{1}{m_Z^4}d_2+\frac{2}{m_Z^2}d_3\right) \tag{B2}$$

$$\frac{1}{4}\sum\left|\mathcal{M}^{(3)}_{SM}\right|^2 = \frac{36e^2m_h^4m_Z^4\left(a_e^2+v_e^2\right)}{v^4\left(q^2-m_Z^2\right)^2}\frac{t_1}{\left(2p_3\cdot p_4+m_h^2\right)^2}\,, \tag{B3}$$

$$\frac{1}{4}\sum\left(\mathcal{M}^{(1)*}_{SM}\mathcal{M}^{(3)}_{SM}+\mathcal{M}^{(1)}_{SM}\mathcal{M}^{(3)*}_{SM}\right) = \frac{24e^2m_h^2m_Z^4\left(a_e^2+v_e^2\right)}{v^4\left(q^2-m_Z^2\right)^2}\frac{t_1}{2p_3\cdot p_4+m_h^2} \tag{B4}$$

$$\frac{1}{4}\sum\left(\mathcal{M}^{(1)*}_{SM}\mathcal{M}^{(2)}_{SM}+\mathcal{M}^{(1)}_{SM}\mathcal{M}^{(2)*}_{SM}\right) = \frac{16e^2m_Z^6\left(a_e^2+v_e^2\right)}{v^4\left(q^2-m_Z^2\right)^2}\left(d_1t_1+\frac{1}{m_Z^2}d_4\right) \tag{B5}$$

$$\frac{1}{4}\sum\left(\mathcal{M}^{(2)*}_{SM}\mathcal{M}^{(3)}_{SM}+\mathcal{M}^{(2)}_{SM}\mathcal{M}^{(3)*}_{SM}\right) = \frac{48e^2m_h^2m_Z^6\left(a_e^2+v_e^2\right)}{v^4\left(q^2-m_Z^2\right)^2}\frac{d_1t_1+\frac{1}{m_Z^2}d_4}{\left(2p_3\cdot p_4+m_h^2\right)}\,. \tag{B6}$$

where we introduced the following kinematic variables:

$$d_1 = \frac{1}{2p_4\cdot p_5+m_h^2}+\frac{1}{2p_3\cdot p_5+m_h^2} \tag{B7}$$

$$d_2 = \frac{t_2}{\left(2p_4\cdot p_5+m_h^2\right)^2}+\frac{t_2^{(3)}}{\left(2p_3\cdot p_5+m_h^2\right)^2}+\frac{2t_3}{\left(2p_4\cdot p_5+m_h^2\right)\left(2p_3\cdot p_5+m_h^2\right)} \tag{B8}$$

$$d_3 = \frac{t_4}{\left(2p_4\cdot p_5+m_h^2\right)^2}+\frac{t_4^{(3)}}{\left(2p_3\cdot p_5+m_h^2\right)^2}+\frac{t_4+t_4^{(3)}}{\left(2p_3\cdot p_5+m_h^2\right)\left(2p_4\cdot p_5+m_h^2\right)} \tag{B9}$$

$$d_4 = \frac{t_4}{2p_4\cdot p_5+m_h^2}+\frac{t_4^{(3)}}{2p_3\cdot p_5+m_h^2} \tag{B10}$$

and

$$t_1 = l_2\cdot(-l_1)+\frac{2\left(l_2\cdot p_5\right)\left((-l_1)\cdot p_5\right)}{m_Z^2} \tag{B11}$$

$$t_2 = \left(2\left(-l_1\right)\cdot\left(p_4+p_5\right)l_2\cdot\left(p_4+p_5\right)-l_2\cdot\left(-l_1\right)\left(p_4+p_5\right)^2\right)\left(-m_h^2+\frac{\left(p_4\cdot p_5\right)^2}{m_Z^2}\right) \tag{B12}$$

$$\begin{aligned} t_3 = {} & \left[\left(-l_1\right)\cdot\left(p_3+p_5\right)l_2\cdot\left(p_4+p_5\right)+\left(-l_1\right)\cdot\left(p_4+p_5\right)l_2\cdot\left(p_3+p_5\right)-l_2\cdot\left(-l_1\right)\left(p_3+p_5\right)\cdot\left(p_4+p_5\right)\right]\times \\ & \times\left(-\left(p_3\cdot p_4\right)+\frac{\left(p_3\cdot p_5\right)\left(p_4\cdot p_5\right)}{m_Z^2}\right) \end{aligned} \tag{B13}$$

$$\begin{aligned} t_4 = {} & 2l_2\cdot\left(p_4+p_5\right)\left(-l_1\right)\cdot\left(p_4+p_5\right)-l_2\cdot\left(-l_1\right)\left(p_4+p_5\right)^2 \\ & -\left[\left(l_2\cdot p_5\right)\left(-l_1\right)\cdot\left(p_4+p_5\right)+\left(-l_1\right)\cdot p_5 l_2\cdot\left(p_4+p_5\right)-l_2\cdot\left(-l_1\right)\left(p_4\cdot p_5+m_Z^2\right)\right]\frac{\left(p_4\cdot p_5+m_Z^2\right)}{m_Z^2} \end{aligned} \tag{B14}$$

$$t_2^{(3)} = t_2\left(p_4\to p_3\right) \tag{B15}$$

$$t_4^{(3)} = t_4\left(p_4\to p_3\right) \tag{B16}$$

Appendix C: Single Higgs production - diagrams

In this Appendix we depict the SM + NP diagrams for $e^+e^- \to hZ$ followed by $Z \to x$ for all $h + x$ channels, (that are calculated by MG5 in section IV) in the presence of $\mathcal{O}_{HL}$. Namely, all diagrams for the processes $e^+e^- \to h\nu_e\overline{\nu}, hl^+l^-, hb\overline{b}$

The full set of diagrams for $e^+e^- \to h\nu_e\overline{\nu}_e$ is:

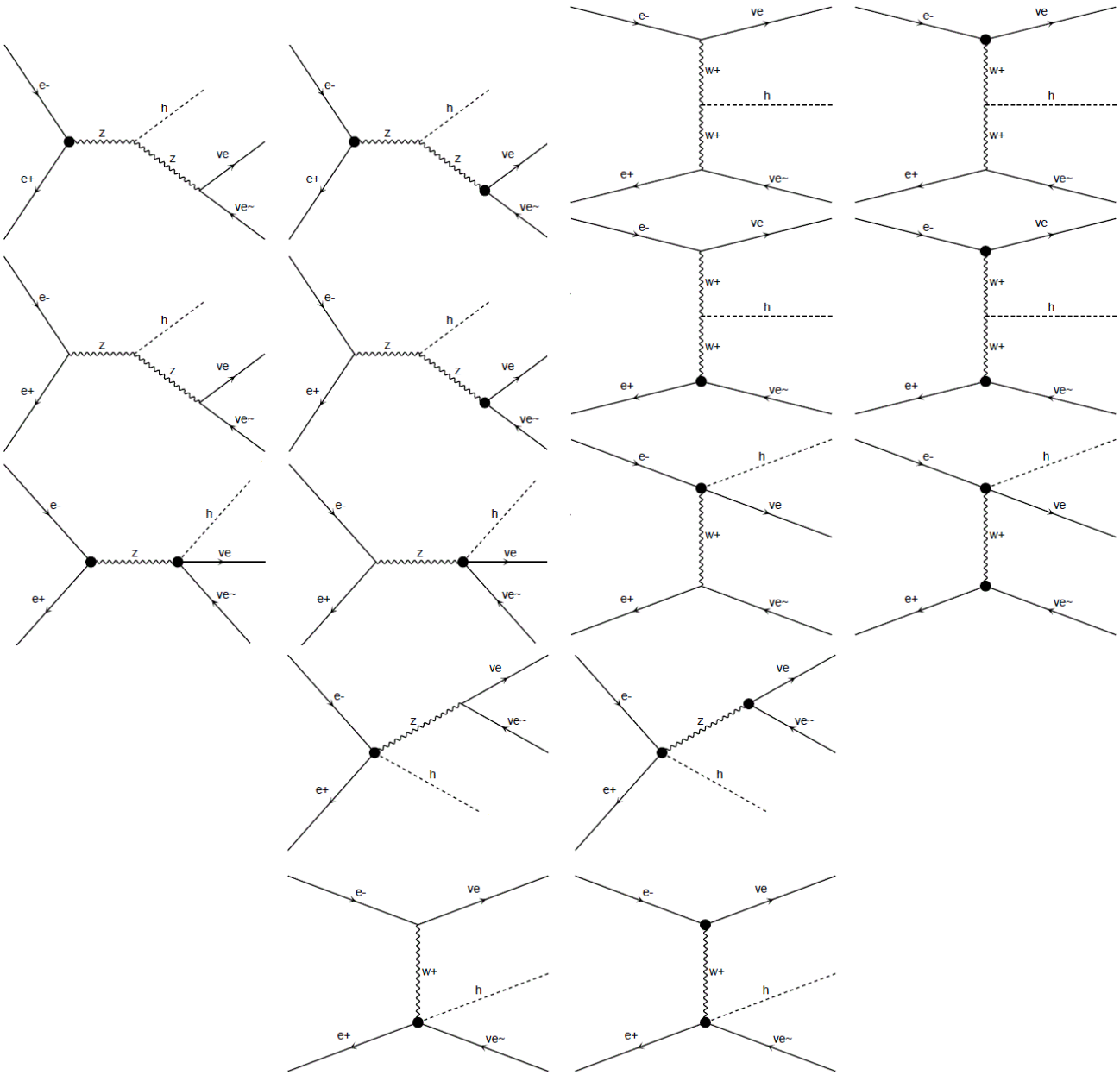

The full set of diagrams for $e^+e^- \to hl^+l^-$ is:

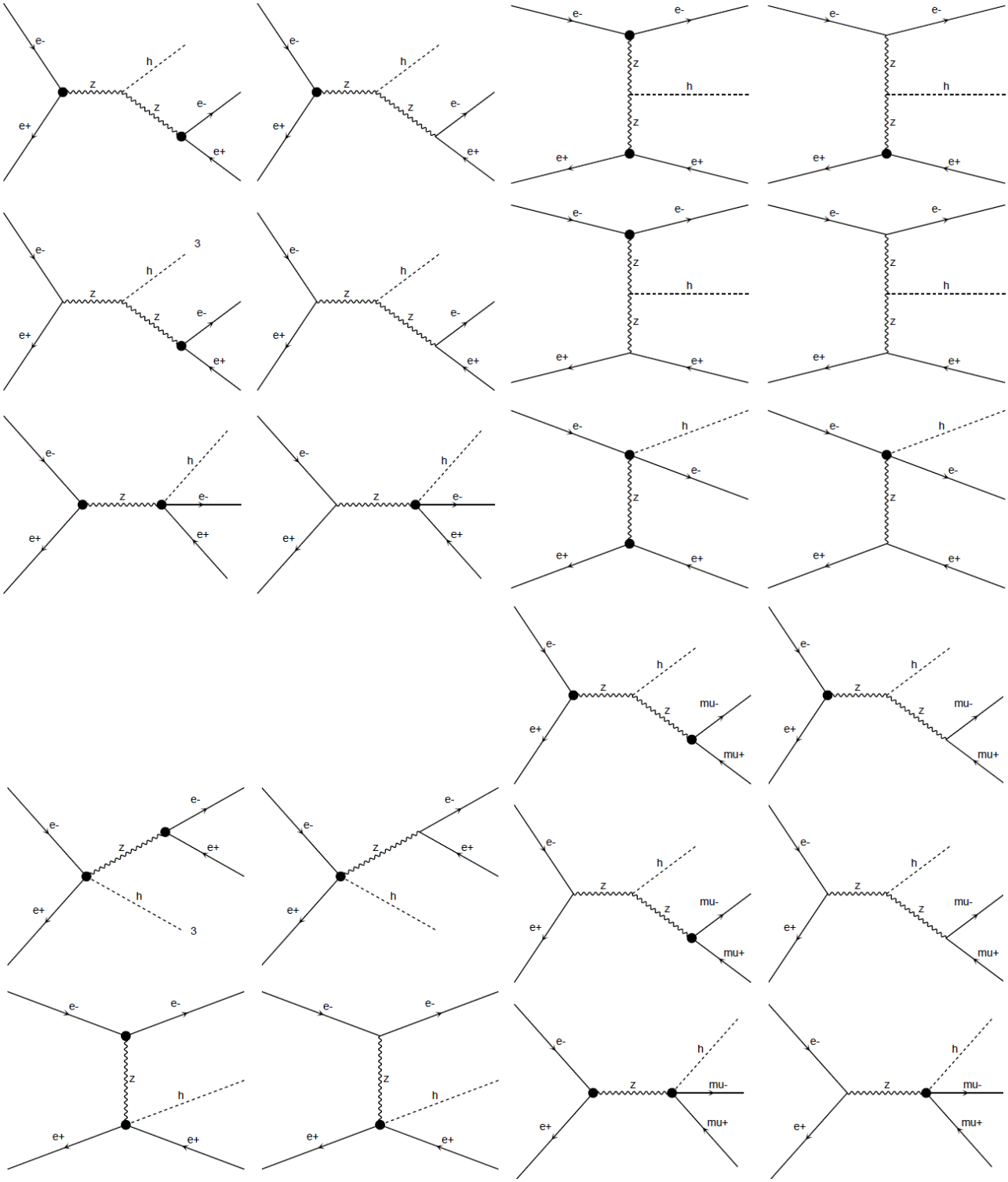

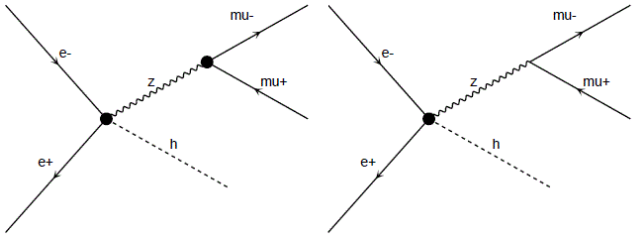

The full set of diagrams for $e^+e^- \to hb\bar{b}$ is:

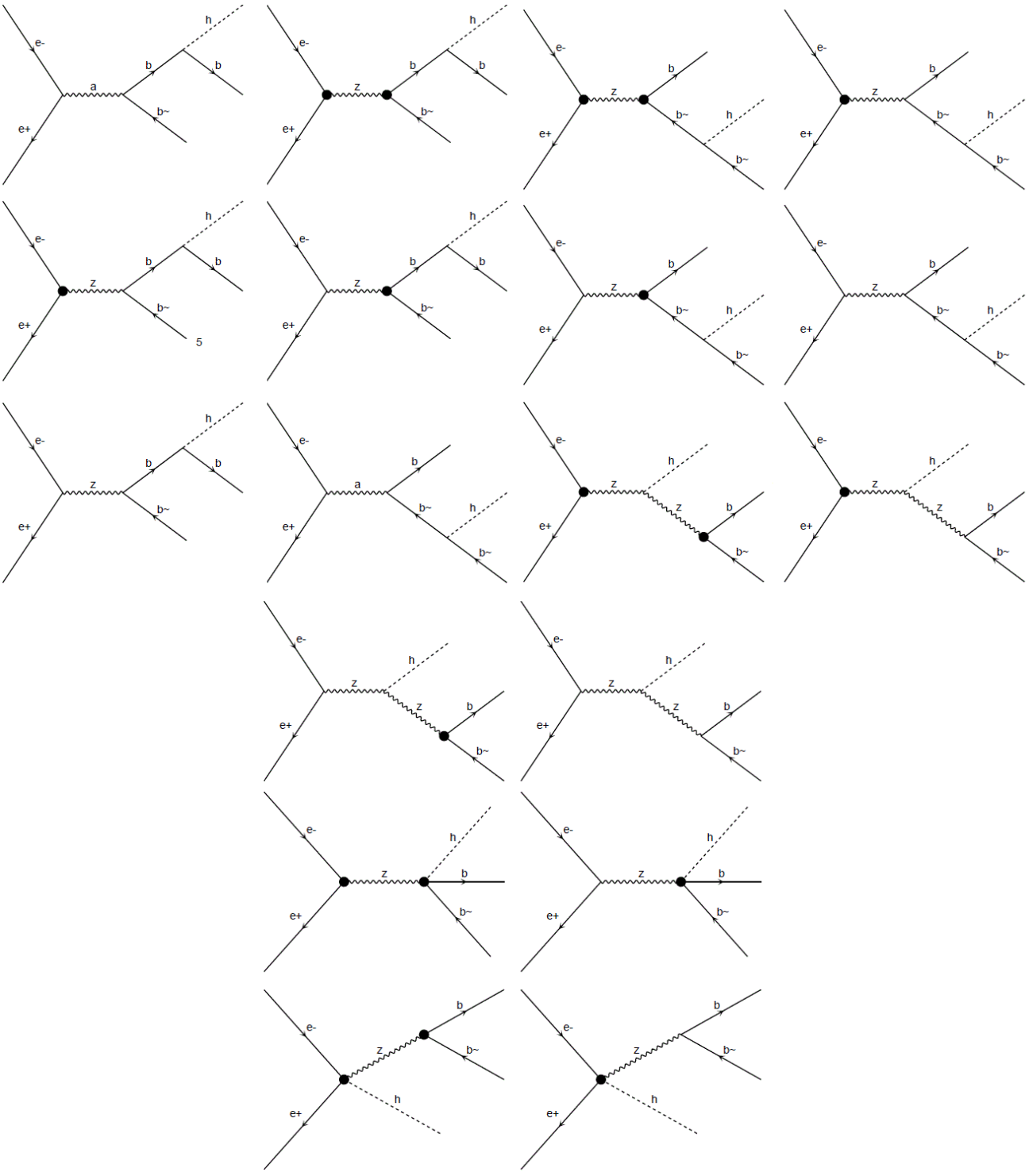

Appendix D: Higgs pair production - sample diagrams

In this Appendix we depict a sample of the SM + NP diagrams for $e^+e^- \to hhZ$ followed by $Z \to x$ for all $hh + x$ channels, (that are calculated by MG5 in section IV) in the presence of $\mathcal{O}_{HL}$. Namely, all diagrams for the processes $e^+e^- \to hh\nu_e\overline{\nu}, hhl^+l^-, hhb\bar{b}$.

A sample of the full set of diagrams for $e^+e^- \to hh\nu_e\overline{\nu}_e$ is:

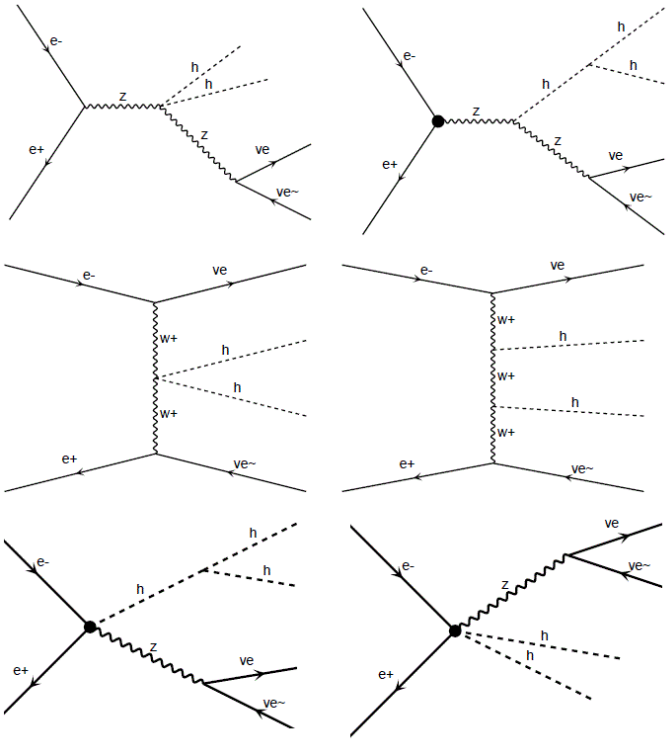

A sample of the full set of diagrams for $e^+e^- \to hhl^+l^-$ is:

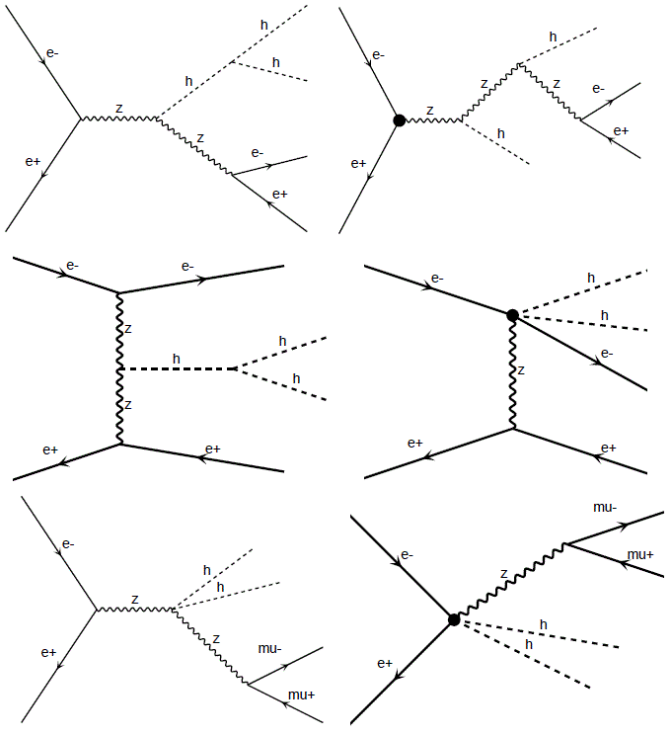

A sample of the full set of diagrams for $e^+e^- \to hhb\bar{b}$ is: